Brief report

Definitive proof for direct reprogramming of hematopoietic cells to pluripotency

*Motohito Okabe,[1] *Makoto Otsu,[1] Dong Hyuck Ahn,[1] Toshihiro Kobayashi,[1] Yohei Morita,[1] Yukiko Wakiyama,[2] Masafumi Onodera,[3] Koji Eto,[1] Hideo Ema,[1] and Hiromitsu Nakauchi[1,2]

[1]Division of Stem Cell Therapy, Center for Stem Cell and Regenerative Medicine, Institute of Medical Science, University of Tokyo, Tokyo; [2]Japan Science and Technology Agency, Exploratory Research for Advanced Technology, Nakauchi Stem Cell and Organ Regeneration Project, Tokyo; and [3]Department of Genetics, National Research Institute for Child Health and Development, Tokyo, Japan

Generation of induced pluripotent stem cells (iPSCs) generally uses fibroblastic cells, but other cell sources may prove useful in both research and clinical settings. Although proof of cellular origin requires genetic-marker identification in both target cells and established iPSCs, somatic cells other than mature lymphocytes mostly lack such markers. Here we show definitive proof of direct reprogramming of murine hematopoietic cells with no rearranged genes. Using iPSC factor transduction, we successfully derived iPSCs from bone marrow progenitor cells obtained from a mouse whose hematopoiesis was reconstituted from a single congenic hematopoietic stem cell. Established clones were demonstrated to be genetically identical to the transplanted single hematopoietic stem cell, thus proving their cellular origin. These hematopoietic cell–derived iPSCs showed typical characteristics of iPSCs, including the ability to contribute to chimerism in mice. These results will prompt further use of hematopoietic cells for iPSC generation while enabling definitive studies to test how cellular sources influence characteristics of descendant iPSCs. (Blood. 2009; 114:1764-1767)

Introduction

Development of induced pluripotent stem cell (iPSC) technology has enabled generation of disease-specific pluripotent stem cells from the patient.[1] A typical method uses virus-mediated transfer of defined factors into fibroblastic cells[2-4] or marrow-derived mesenchymal cells.[1,5] Some other tissues are also reported as sources for iPSC generation, including murine hepatocytes and gastric epithelial cells,[6] human keratinocytes,[7] and very recently, human blood.[8] As the variability of cellular sources becomes greater, it is attractive to address an interesting question: is each iPSC clone derived from distinct sources unique in its characteristics? Although definitive proof of iPSC cellular origin requires genetic markers, as most somatic cells (except mature lymphocytes) lack such markers, no formal data have shown reprogramming of hematopoietic cells, aside from one study that used immunoglobulin genes as markers.[9] Here, we demonstrate definitive proof for a direct reprogramming to pluripotency of primary marrow hematopoietic cells with no gene rearrangement.

Methods

Mice

Animal experiments were performed with approval of the Institutional Animal Care and Use Committee of the Institute of Medical Science, University of Tokyo.

Generation of iPSCs from murine bone marrow progenitor cells

Lineage marker–negative (Lin^-) c-Kit^+ (Kit^+) cells were enriched using immunomagnetic beads. pMXs vectors[10] encoding iPSC genes are described.[1] Concentrated vesicular stomatitis virus-G–retroviral supernatant was prepared using reported procedures.[11-13] 293GP and 293GPG cells were kind gifts from Dr R. C. Mulligan (Children's Hospital Boston, Harvard Medical School, Boston, MA).[14] Detailed procedures are described in the text and supplemental data (available on the *Blood* website; see the Supplemental Materials link at the top of the online article).

In vitro and in vivo assessment of iPSCs

Characteristics of iPSCs were assessed following reported procedures.[1] Primer sequences are shown in supplemental Table 1. Immunoglobulin heavy chain gene rearrangement was analyzed following described methods.[15,16] A single-base difference within *Cd45* exon 25 was analyzed as reported.[17]

Results and discussion

To prove the cellular origin of iPSC clones formally, use of definitive genetic markers is necessary, as with reported reprogramming of mature B cells[9] and pancreatic beta cells.[18] Even if iPSCs are generated from hematopoietic stem/progenitor cells (HSPCs), nearly 100% positive for the hematopoietic marker CD45, one might argue, in light of reported generation of iPSCs from marrow stromal cells,[1,5] that a small number of nonhematopoietic cells had been reprogrammed. However, no such suitable marker exists for hematopoietic cells (excepting rearranged immunoreceptor genes in mature lymphocytes). We therefore exploited a prominent characteristic of the hematopoietic system: transplantation of a single hematopoietic stem cell (HSC) can reconstitute host hematopoiesis.[19]

Submitted February 4, 2009; accepted May 11, 2009. Prepublished online as *Blood* First Edition paper, June 29, 2009; DOI 10.1182/blood-2009-02-203695.

*M. Okabe and M. Otsu contributed equally to this work.

The online version of this article contains a data supplement.

The publication costs of this article were defrayed in part by page charge payment. Therefore, and solely to indicate this fact, this article is hereby marked "advertisement" in accordance with 18 USC section 1734.

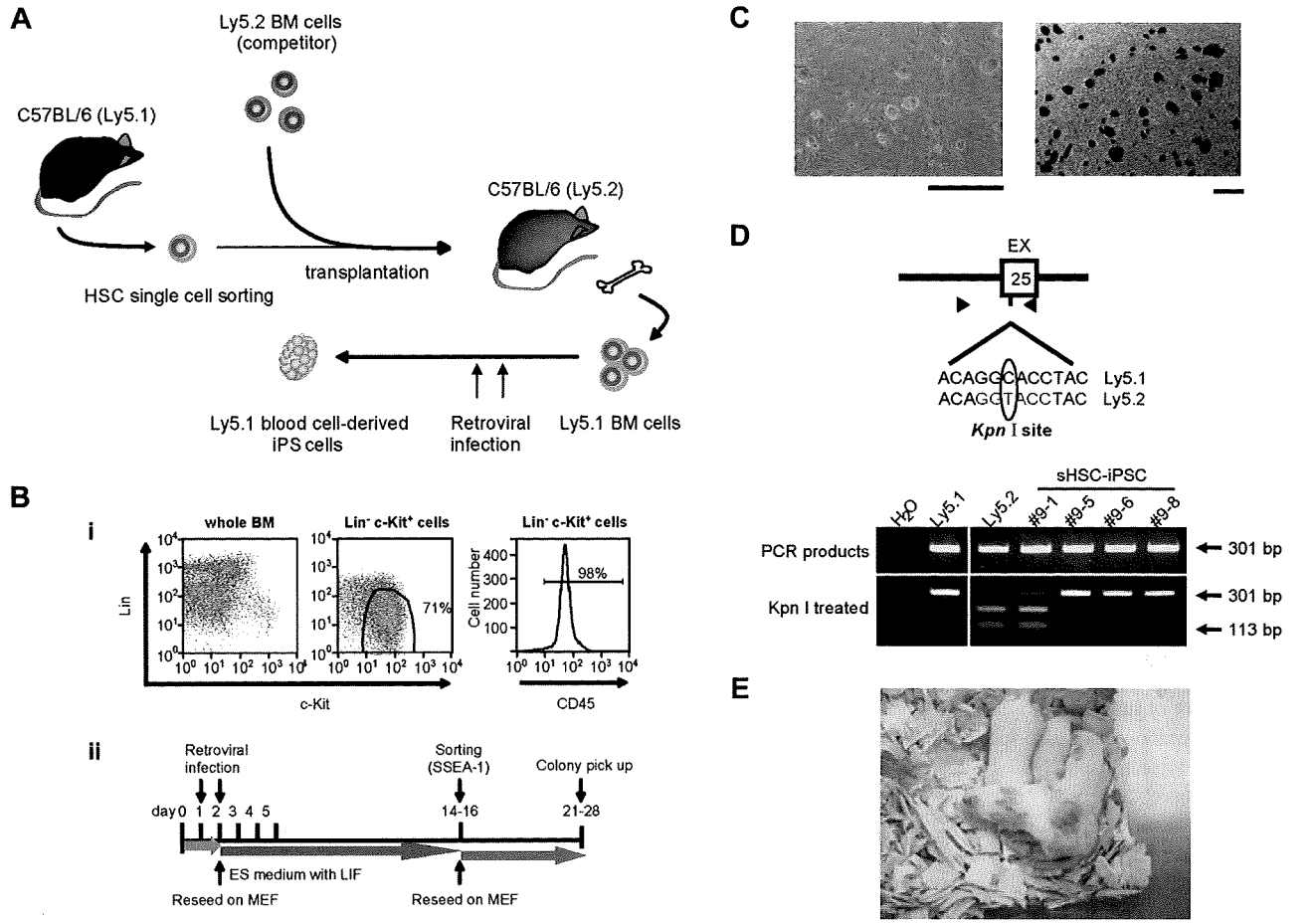

Figure 1. Proof of iPSC induction from hematopoietic cells in a single-HSC transplantation model. (A) Schematic representation of the experimental procedure. Single $CD150^{+}CD34^{-/low}$ KSL cells obtained from B6 Ly5.1 mice were transplanted into lethally irradiated B6 Ly5.2 mice together with BM cells from B6 Ly5.2 mice. BM HSPCs were obtained from a recipient mouse that showed long-term (~ 10 months) stable Ly5.1 chimerism (~ 80%), enriched for $Ly5.1^{+}$ cells, and subjected to iPSC generation. (B) A schematic diagram of iPSC generation from BM HSPCs. (i) Lineage markers (Lin) versus c-Kit plots are shown for cells either before (whole BM) or after ($Lin^{-}c\text{-}Kit^{+}$) purification. Note that purified HSPCs are 98% CD45-positive. (ii) A schematic diagram of iPSC generation from BM HSPCs. (C) Typical ES cell–like appearance of sHSC-iPS cell colonies (left) with high ALP activities (right). Bars represent 100 μm. (D) Determination of the cellular origin of sHSC-iPSC clones. (Top panel) Scheme of the polymerase chain reaction (PCR)–based method used, using a single-base polymorphism at *Cd45* exon (EX) 25. Black triangles represent primer positions. Ly5.1 and Ly5.2 strains differ by a single base in EX 25, as shown in the presented 12-bp sequences from within the 301-bp amplicons. Treatment with the restriction enzyme *Kpn*I leaves the $Ly5.1^{+}$ cell–derived amplicon undigested, whereas it generates 2 smaller fragments (113 bp + 188 bp) from the $Ly5.2^{+}$ counterpart. The gel images (bottom panel) indicate that, of 4 sHSC-iPSC clones, 1 (no. 9-1) is of $Ly5.2^{+}$ cell origin, whereas 3 (nos. 9-5, -6, and -8) are derived from $Ly5.1^{+}$ cells that originated from a single $Ly5.1^{+}$ HSC. A vertical line has been inserted to indicate a repositioned gel lane. (E) Chimeric mice obtained by implantation of sHSC-iPSC clone 9-5 into ICR host blastocysts.

Figure 1A depicts our experimental design. We attempted iPSC generation from marrow HSPCs harvested long-term (~ 10 months) after reconstitution from a single HSC of C57BL6 (B6) Ly 5.1 origin. We used concentrated vesicular stomatitis virus-G–pseudotyped retroviruses,[14] as we had succeeded in their efficient transduction into murine HSPCs.[12,13] We purified from bone marrow (BM) of a reconstituted mouse (B6 Ly5.2) $Lin^{-}Kit^{+}$ cells, a HSPC population, with approximately 98% of cells expressing CD45 (Figure 1B). We then transduced these cells with a cocktail of retroviral vectors harboring each of the iPSC factor genes *Oct4*, *Sox2*, *Klf4*, and *c-Myc*, transferred onto mouse embryonic fibroblast cells, and maintained in the presence of leukemia inhibitory factor until cell sorting (Figure 1B). Visible iPSC-like colonies appeared on approximately days 9 to 11 among a majority of hematopoietic cells that remained nonreprogrammed; these colonies then grew steadily (supplemental Figure 1A). To enrich iPSC candidates, we sorted the cells expressing SSEA-1 on approximately days 14 to 16 and allowed them to regrow for another 7 to 12 days (Figure 1B). Generated iPSC-like colonies showing typical embryonic stem (ES) cell–like appearance were picked up on approximately days 21 to 28. These cells showed robust stability in phenotype, had high alkaline phosphatase (ALP) activity (Figure 1C), and expressed SSEA-1 at levels comparable with those in ES cells (supplemental Figure 1B). In the absence of leukemia inhibitory factor, they readily formed embryoid bodies (data not shown). By using a single-base polymorphism in *CD45*,[17] we could demonstrate that, of the iPSC clones thus established, 3 were derived from $Ly5.1^{+}$ cells and 1 from a $Ly5.2^{+}$ cell (Figure 1D). These results formally demonstrate that direct reprogramming of marrow hematopoietic cells is feasible given that transdifferentiation of HSCs to nonhematopoietic lineage cells is, if it ever occurs, an extremely rare event.[20] We named these iPSCs sHSC-iPS cells (sHSC-iPSCs) specifically when established from BM HSPCs reconstituted from a single HSC.

Each sHSC-iPSC clone was demonstrated to retain proviral sequences of the 4 iPSC factors (supplemental Figure 2A), without detectable transgene expression, probably resulting from gene silencing (supplemental Figure 2B). In contrast, all sHSC-iPSCs were found to express each iPSC factor gene endogenously (supplemental Figure 2B). All sHSC-iPSCs were shown to express the ES cell marker genes *Nanog*, *ERas*, *Rex1*, and *Gdf3* (supplemental Figure 3A). Nanog expression was also confirmed by immunostaining (supplemental Figure 3B). Despite the low expression levels of *Ecat1* and *Zfp296*, another set of ES cell marker genes, these sHSC-iPSCs were shown to

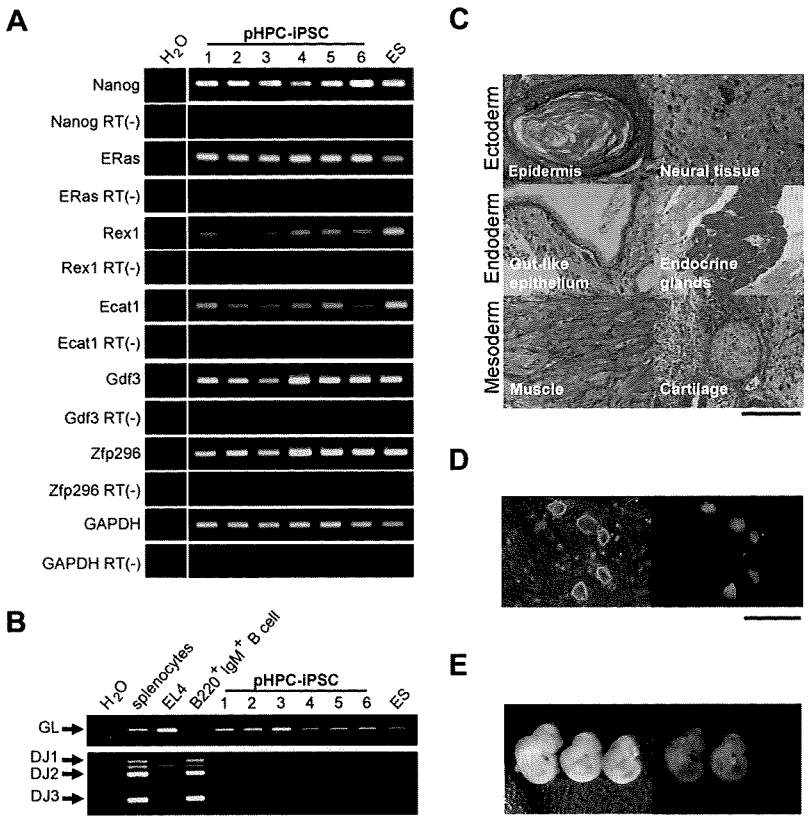

Figure 2. Characterization of primary BM hematopoietic cell–derived iPSCs generated using the 4 iPSC factors. (A) Reverse-transcription PCR analysis showing ES marker gene expression in primary BM HSPC-derived iPSC clones (pHPC-iPSCs). H_2O indicates no-template control; ES, ES cells as a positive control; RT (−), no-reverse-transcriptase control. A vertical line has been inserted to indicate a repositioned gel lane. (B) PCR analysis for Ig gene rearrangement of D-J segments (DJ1-DJ3) in pHPC-iPSC clones. GL indicates amplification of the fragment representing unrearranged, germline configuration of the Ig heavy chain gene; EL4, a T lymphoma cell line as an unrearranged control. (C) Histologic sections of teratomas derived from a pHPC-iPSC clone. (D) Images of pHPC-iPSC colonies derived from an EGFP-transgenic mouse. Bars represent 100 μm (C-D). (E) E10.5 chimeric embryos generated with one representative $EGFP^+$ iPSC clone.

be competent in both teratoma formation (supplemental Figure 4) and contribution to chimeric mice (Figure 1E).

We next sought to confirm the reproducibility of direct reprogramming of primary BM HSPCs. Lin^-Kit^+ BM cells obtained from adult B6 mice were subjected to retrovirus-mediated reprogramming procedures (Figure 1B). From approximately 5×10^5 HSPCs, we consistently obtained approximately 10 to 30 discrete colonies with typical ES cell–like appearances that stained for ALP (data not shown). Interestingly, iPSC clones established from primary BM HSPCs (pHPC-iPSCs) were shown to express ES cell marker genes more robustly than did sHSC-iPSCs (Figures 2A, S3A). Expression levels in endogenous iPSC factor genes were also more intense in pHPC-iPSCs (supplemental Figure 5B) than in sHSC-iPSCs (supplemental Figure 2B). This may support the idea that huge replicative stress imposed on a single HSC by hematopoietic reconstitution might restrict effective reprogramming of target cells, which are thought to be in senescent states. Confirmation of germline configuration in the immunoglobulin gene revealed the non–B-cell origin of pHPC-iPSCs (Figure 2B). pHPC-iPSCs had the potential for multilineage differentiation, as evidenced by the formation of teratomas, which contained various tissues representing all 3 germ layers (Figure 2C). We were also successful in generating pHPC-iPSCs that constitutively expressed green fluorescence protein from enhanced green fluorescent protein (EGFP)–transgenic mice[21] (Figure 2D). These iPSCs showed a high contribution to embryonic development when microinjected into blastocysts (Figure 2E).

Here we report generation of iPSCs from hematopoietic cells with unrearranged immunoreceptor genes by direct viral transfer of iPSC factors. The principle shown here ensures the feasibility of direct reprogramming of human hematopoietic cells, in conjunction with the recent report of iPSC generation from human blood.[8] The defined cellular origin of our iPSCs enables formal comparative studies using iPSC clones from various sources: One intriguing question is whether or not our iPSC clones differ from those generated from other tissues in respect to reprogramming efficiency, genomic stability, ability of tissue differentiation, and susceptibility to tumorigenesis. Another question is what types of cells in murine HSPCs are actually reprogrammed into iPSCs. At present, we have not yet succeeded in iPSC generation from highly purified HSCs. Considering the germline configuration of the immunoglobulin gene in our iPSC clones (Figure 2B) and the fact that the transduced cells rapidly acquired granulocytic/myeloid-lineage marker expression in our culture conditions (data not shown), myeloid progenitors are currently the plausible target cells of iPSC induction in our system. Studies to address all these issues are ongoing.

Acknowledgments

The authors thank S. Yamanaka and K. Takahashi for plasmids, R. C. Mulligan for 293GP and 293GPG cells, and H. Kawamoto and T. Ikawa for help with Ig gene analysis.

This work was supported in part by a grant from the Project for Realization of Regenerative Medicine from the Ministry of Education, Culture, Sports, Science and Technology Japan (H.N.) and by the Global Center of Excellence program from the Ministry of Education, Culture, Sports, Science and Technology Japan.

Authorship

Contribution: M. Okabe generated and characterized iPS cells; M. Otsu generated iPS cells and wrote the manuscript; D.H.A. prepared virus-producing cells; T.K. and Y.W. performed blastocyst injection; Y.M. prepared a single HSC-transplanted chimeric mouse; M. Onodera established transduction procedures

using 293GPG cells; K.E. and H.E. supported experiments with their professional knowledge and experience; and M. Otsu and H.N. supervised the study.

Conflict-of-interest disclosure: The authors declare no competing financial interests.

Correspondence: Hiromitsu Nakauchi, Division of Stem Cell Therapy, Center for Stem Cell and Regenerative Medicine, Institute of Medical Science, University of Tokyo, 4-6-1 Shirokanedai Minato-ku, 108-8639 Tokyo, Japan; e-mail: nakauchi@ims.u-tokyo.ac.jp.

References

1. Takahashi K, Yamanaka S. Induction of pluripotent stem cells from mouse embryonic and adult fibroblast cultures by defined factors. *Cell.* 2006; 126:663-676.
2. Wernig M, Meissner A, Foreman R, et al. In vitro reprogramming of fibroblasts into a pluripotent ES-cell-like state. *Nature.* 2007;448:318-324.
3. Takahashi K, Okita K, Nakagawa M, Yamanaka S. Induction of pluripotent stem cells from fibroblast cultures. *Nat Protoc.* 2007;2:3081-3089.
4. Yu J, Vodyanik MA, Smuga-Otto K, et al. Induced pluripotent stem cell lines derived from human somatic cells. *Science.* 2007;318:1917-1920.
5. Park IH, Arora N, Huo H, et al. Disease-specific induced pluripotent stem cells. *Cell.* 2008;134: 877-886.
6. Aoi T, Yae K, Nakagawa M, et al. Generation of pluripotent stem cells from adult mouse liver and stomach cells. *Science.* 2008;321:699-702.
7. Aasen T, Raya A, Barrero MJ, et al. Efficient and rapid generation of induced pluripotent stem cells from human keratinocytes. *Nat Biotechnol.* 2008; 26:1276-1284.
8. Loh YH, Agarwal S, Park IH, et al. Generation of induced pluripotent stem cells from human blood. *Blood.* 2009;113:5476-5479.
9. Hanna J, Markoulaki S, Schorderet P, et al. Direct reprogramming of terminally differentiated mature B lymphocytes to pluripotency. *Cell.* 2008;133: 250-264.
10. Onishi M, Kinoshita S, Morikawa Y, et al. Applications of retrovirus-mediated expression cloning. *Exp Hematol.* 1996;24:324-329.
11. Hamanaka S, Nabekura T, Otsu M, et al. Stable transgene expression in mice generated from retrovirally transduced embryonic stem cells. *Mol Ther.* 2007;15:560-565.
12. Nabekura T, Otsu M, Nagasawa T, Nakauchi H, Onodera M. Potent vaccine therapy with dendritic cells genetically modified by the gene-silencing-resistant retroviral vector GCDNsap. *Mol Ther.* 2006;13:301-309.
13. Sanuki S, Hamanaka S, Kaneko S, et al. A new red fluorescent protein that allows efficient marking of murine hematopoietic stem cells. *J Gene Med.* 2008;10:965-971.
14. Ory DS, Neugeboren BA, Mulligan RC. A stable human-derived packaging cell line for production of high titer retrovirus/vesicular stomatitis virus G pseudotypes. *Proc Natl Acad Sci U S A.* 1996;93: 11400-11406.
15. Kawamoto H, Ikawa T, Ohmura K, Fujimoto S, Katsura Y. T cell progenitors emerge earlier than B cell progenitors in the murine fetal liver. *Immunity.* 2000;12:441-450.
16. Schlissel MS, Corcoran LM, Baltimore D. Virus-transformed pre-B cells show ordered activation but not inactivation of immunoglobulin gene rearrangement and transcription. *J Exp Med.* 1991; 173:711-720.
17. Ramos CA, Zheng Y, Colombowala I, Goodell MA. Tracing the origin of non-hematopoietic cells using CD45 PCR restriction fragment length polymorphisms. *Biotechniques.* 2003;34:160-162.
18. Stadtfeld M, Brennand K, Hochedlinger K. Reprogramming of pancreatic beta cells into induced pluripotent stem cells. *Curr Biol.* 2008;18:890-894.
19. Osawa M, Hanada K, Hamada H, Nakauchi H. Long-term lymphohematopoietic reconstitution by a single CD34-low/negative hematopoietic stem cell. *Science.* 1996;273:242-245.
20. Wagers AJ, Sherwood RI, Christensen JL, Weissman IL. Little evidence for developmental plasticity of adult hematopoietic stem cells. *Science.* 2002;297:2256-2259.
21. Okabe M, Ikawa M, Kominami K, Nakanishi T, Nishimune Y. "Green mice" as a source of ubiquitous green cells. *FEBS Lett.* 1997;407:313-319.

nature medicine

$CD8^+$ effector T cells contribute to macrophage recruitment and adipose tissue inflammation in obesity

Satoshi Nishimura[1–4], Ichiro Manabe[1,2,4,5], Mika Nagasaki[1,6], Koji Eto[7], Hiroshi Yamashita[1], Mitsuru Ohsugi[8], Makoto Otsu[7], Kazuo Hara[8], Kohjiro Ueki[3,5,8], Seiryo Sugiura[9], Kotaro Yoshimura[10], Takashi Kadowaki[3,5,8] & Ryozo Nagai[1,3,5]

Inflammation is increasingly regarded as a key process underlying metabolic diseases in obese individuals. In particular, obese adipose tissue shows features characteristic of active local inflammation. At present, however, little is known about the sequence of events that comprises the inflammatory cascade or the mechanism by which inflammation develops. We found that large numbers of $CD8^+$ effector T cells infiltrated obese epididymal adipose tissue in mice fed a high-fat diet, whereas the numbers of $CD4^+$ helper and regulatory T cells were diminished. The infiltration by $CD8^+$ T cells preceded the accumulation of macrophages, and immunological and genetic depletion of $CD8^+$ T cells lowered macrophage infiltration and adipose tissue inflammation and ameliorated systemic insulin resistance. Conversely, adoptive transfer of $CD8^+$ T cells to CD8-deficient mice aggravated adipose inflammation. Coculture and other *in vitro* experiments revealed a vicious cycle of interactions between $CD8^+$ T cells, macrophages and adipose tissue. Our findings suggest that obese adipose tissue activates $CD8^+$ T cells, which, in turn, promote the recruitment and activation of macrophages in this tissue. These results support the notion that $CD8^+$ T cells have an essential role in the initiation and propagation of adipose inflammation.

Inflammation is now considered to have a pivotal role in the development of metabolic diseases[1]. In particular, obese adipose tissue shows the hallmarks of chronic inflammation[2,3], and the inflammation is thought to alter adipose tissue function, leading to systemic insulin resistance[4]. The mechanism by which the development of this insulin resistance occurs is believed to involve proinflammatory cytokines produced by infiltrating macrophages and resident adipocytes within the obese adipose tissue[1]. Likewise, chronic inflammation also impairs triglyceride storage in adipose tissues, and the excess circulating free fatty acids and triglycerides also induces insulin resistance in muscle and liver[5–7]. Adding insult to injury, it has been postulated that a paracrine loop involving these free fatty acids and inflammatory cytokines establishes a vicious cycle that aggravates the inflammatory changes, furthering the dysfunction of adipose tissue[8]. As such, the inflammatory changes seen in obese adipose tissue may be the key pathology that promotes systemic inflammatory states and insulin resistance in obese individuals.

Macrophage infiltration of adipose tissue has been described in both mice and humans[1]. However, little is known about the sequence of events that lead to macrophage infiltration. Recently accumulation of other immune cells, such as T cells, has been documented in obese adipose tissue[9,10]. T lymphocytes are known to interact with macrophages and regulate the inflammatory cascade[11]. However, their functional role in adipose inflammation remains unclear. Here we show that infiltration of $CD8^+$ effector T cells is an early event during the development of adipose tissue obesity induced by a high-fat diet. Further, we show using loss- and gain-of-function approaches *in vivo* that these T cells are critical mediators of systemic metabolic dysfunction. Finally, we also show *in vitro* that obese adipose tissue can activate $CD8^+$ T cells, which, in turn, allows for the recruitment and differentiation of macrophages. Thus, together our findings indicate that $CD8^+$ T cells have essential roles in the initiation and maintenance of adipose tissue inflammation and systemic insulin resistance. Our results also clearly show the involvement of adaptive immunity in metabolic disorders.

RESULTS

$CD8^+$ T cell infiltration precedes macrophage accumulation

Adipose tissue consists of not only adipocytes but also stromal and vascular cells, including fibroblasts, vascular endothelial cells and inflammatory cells. This stromal vascular fraction is known to be essential for adipose tissue inflammation[2]. Therefore, to gain insight

[1]Department of Cardiovascular Medicine, [2]Nano-Bioengineering Education Program and [3]Translational Systems Biology and Medicine Initiative, Graduate School of Medicine, The University of Tokyo, Tokyo, Japan. [4]PRESTO, Japan Science and Technology Agency, Kawaguchi, Japan. [5]Comprehensive Center of Education and Research for Chemical Biology of the Diseases, [6]Computational Diagnostic Radiology and Preventive Medicine, The University of Tokyo, Tokyo, Japan. [7]Division of Stem Cell Therapy, Center for Stem Cell Biology and Regenerative Medicine, Institute of Medical Science, The University of Tokyo, Tokyo, Japan. [8]Department of Metabolic Diseases, Graduate School of Medicine, The University of Tokyo, Tokyo, Japan. [9]Department of Human and Engineered Environmental Studies, Graduate School of Frontier Sciences, The University of Tokyo, Tokyo, Japan. [10]Department of Plastic Surgery, Graduate School of Medicine, The University of Tokyo, Tokyo, Japan. Correspondence should be addressed to S.N. (snishi-tky@umin.ac.jp) or I.M. (manabe-tky@umin.ac.jp).

Received 5 January; accepted 7 April; published online 26 July 2009; doi:10.1038/nm.1964

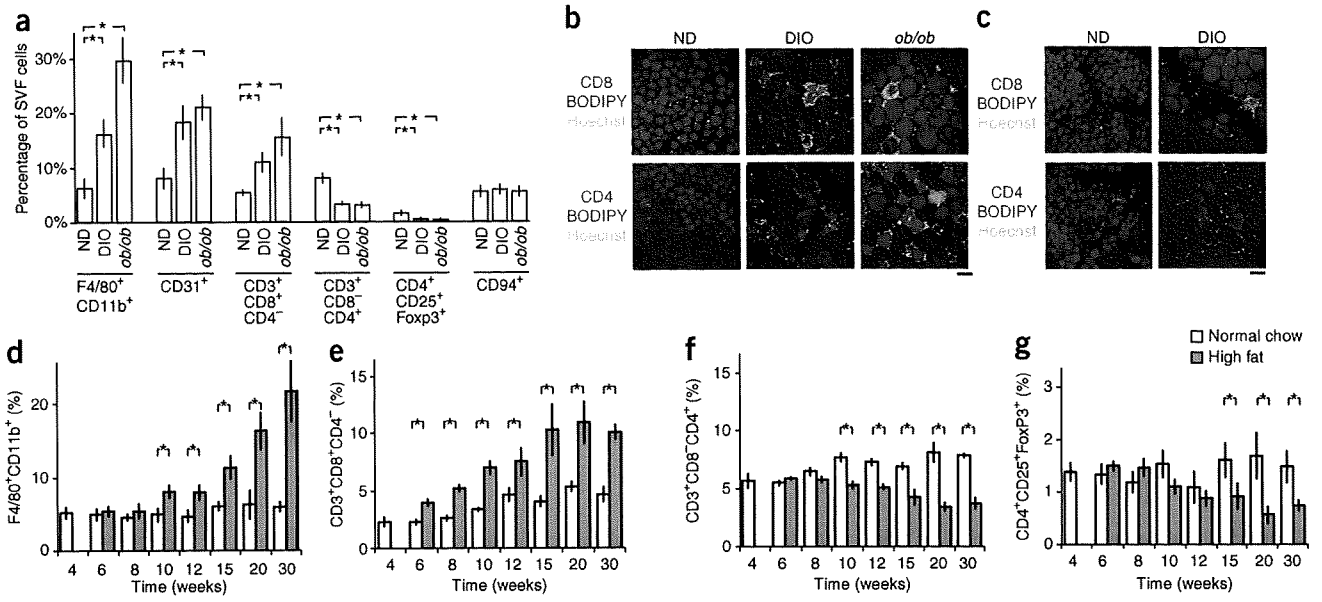

Figure 1 Differential infiltration of lymphocytes and macrophages into obese adipose tissue. (**a**) Flow cytometric analysis of the stromal vascular fraction (SVF) from the epididymal fat pads of control mice fed a normal chow diet (ND), diet-induced obese (DIO) mice fed a high-fat diet for 16 weeks and *ob/ob* mice fed a normal diet (*ob/ob*). All mice were 20-weeks-old. The cell populations of macrophages ($F4/80^+CD11b^+$), endothelial cells ($CD31^+$), $CD3^+CD8^+CD4^-$ T cells, $CD3^+CD8^-CD4^+$ T cells, regulatory T cells ($CD4^+CD25^+Foxp3^+$) and NK cells ($CD3^-CD94^+$) were analyzed ($n = 5$ mice in each group). The number of each cell type was normalized to the total number of viable SVF cells. $^*P < 0.05$. (**b,c**) Immunohistochemical analysis of CD8 and CD4 (each in red) in epididymal (**b**) and femoral subcutaneous (**c**) adipose tissue from ND, DIO and *ob/ob* mice. Adipocytes were counterstained with boron-dipyrromethene (BODIPY, blue) and nuclei with Hoechst (green). Quantification of $CD8^+$ and $CD4^+$ cells is shown in **Supplementary Fig. 3**. Scale bars, 100 μm. (**d–g**) Time courses of changes in the cell populations in the adipose stroma during development of obesity. Flow cytometric analysis of the stromal vascular fraction from the epididymal fat pads of control mice fed a normal chow diet and mice fed a high-fat diet beginning when they were 4-weeks-old. Numbers of macrophages (**d**), $CD8^+$ T cells (**e**), $CD4^+$ T cells (**f**) and regulatory T cells (**g**) were determined during the course of DIO development ($n = 5$ mice in each group; $^*P < 0.05$). Error bars represent means ± s.e.m.

into the inflammatory processes taking place within these cell fractions during obesity, we first analyzed immune cell populations in collagenase-digested stromal vascular fractions from obese epididymal adipose tissue with the aim of identifying local obesity-induced immunological changes. We acquired stromal vascular fractions using previously described methods of isolation[12] with a few modifications. We first carried out a set of flow cytometric analyses to determine the proper gating for analysis of lymphocytes and macrophages in adipose tissue (**Supplementary Fig. 1**). We found that R1 gating accounted for the majority of viable cells, including a majority of $F4/80^+CD11b^+$ macrophages. Because earlier studies used broader gating to analyze macrophages in the stromal vascular fraction[13], we compared the broader R2 gating with the narrower R1 gating. We found that the macrophage and lymphocyte fractions detected with R1 gating did not significantly differ from those detected using the broader R2 gating (**Supplementary Fig. 1** and **Supplementary Table 1**). For that reason, we analyzed subsequent cell fractions by R1 gating (for further discussion of gating, see **Supplementary Methods** and **Supplementary Fig. 1**).

Consistent with earlier reports[2], the infiltration of $F4/80^+CD11b^+$ macrophages into adipose tissue was significantly increased by diet-induced obesity (DIO) and in obese *ob/ob* mice compared to the control lean mice on a normal diet ($P < 0.05$) (**Fig. 1a**). The numbers of $CD31^+$ endothelial cells were also higher in obese mice (**Fig. 1a**), which may reflect angiogenesis[14]. Notably, we found that $CD3^+$ T cells accounted for 14.8 ± 0.9% of stromal vascular cells in lean adipose tissue, and most (94.7 ± 0.3%) of the $CD3^+$ T cells were CD4 or CD8 positive. The $CD3^+CD8^+CD4^-$ T cell fraction was larger in obese adipose tissue, whereas the $CD3^+CD4^+CD8^-$ T cell fraction was smaller, as was the regulatory T cell fraction ($CD4^+CD25^+Foxp3^+$) compared to lean mice on normal diet ($P < 0.05$). The natural killer (NK) cell fraction ($CD3^-CD94^+$) was unaffected by obesity (**Fig. 1a**). In contrast to the higher number of $CD8^+$ lymphocytes seen in obese adipose tissue, $CD8^+$ and $CD4^+$ T cell counts were significantly lower in peripheral blood from *ob/ob* mice and were unchanged in DIO mice as compared to mice on a normal diet ($P < 0.05$) (**Supplementary Fig. 2**), suggesting selective recruitment of $CD8^+$ T lymphocytes to obese adipose tissues.

Immunohistochemical analysis of F4/80, CD8 and CD4 expression also revealed higher numbers of $F4/80^+$ macrophages and $CD8^+$ T cells and lower numbers of $CD4^+$ T cells in obese epididymal fat pads as compared to mice on a normal diet ($P < 0.05$) (**Fig. 1b** and **Supplementary Fig. 3**). By contrast, we found no significant changes in the numbers of $CD8^+$ and $CD4^+$ cells in subcutaneous fat pads (**Fig. 1c**). In obese epididymal adipose tissues, we found a number of $CD8^+$ cells within 'crown-like structures' (CLSs), which reflect the focal convergence of macrophages surrounding necrotic adipocytes[14,15] (**Fig. 1b**), whereas $CD4^+$ cells showed no apparent relationship with CLSs.

Most $CD3^+CD8^+$ cells were $CD62L^-$ and $CD44^+$ (74.7% ± 3.8% of $CD3^+$ $CD8^+$ cells in DIO mice), suggesting the majority of infiltrated $CD8^+$ T cells were activated effector T cells[16]. To assess the clonality of $CD8^+$ in obese adipose, we examined the T cell receptor (TCR) V_β repertoire of $CD8^+$ T cells in lean and obese adipose tissues. The results showed that $CD8^+$ T cells in obese adipose were not monoclonal, though the $CD8^+$ cell fractions that were positive for $V_{\beta 7}$ and $V_{\beta 20b}$ were significantly larger in obese adipose tissues as compared to mice on a normal diet ($P < 0.05$) (**Supplementary Fig. 4**).

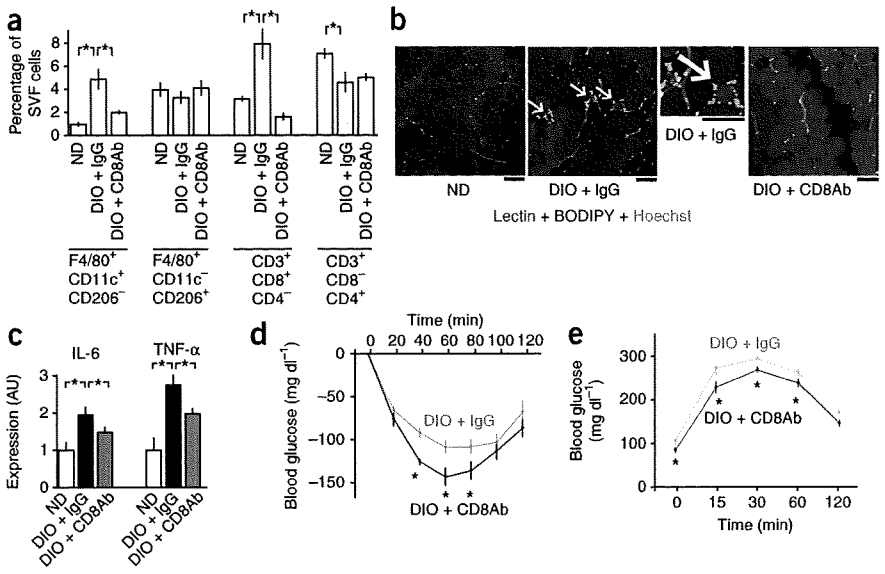

Figure 2 Effects of CD8-specific antibody treatment on obese adipose tissue inflammation. (**a**) Flow cytometric analysis of M1 macrophages ($F4/80^+CD11c^+CD206^-$), M2 macrophages ($F4/80^+CD11c^-CD206^+$), $CD8^+$ T cells and $CD4^+$ T cells in stromal vascular fractions in mice from lean normal-diet (ND), and DIO mice administered either antibody to CD8 (DIO + CD8Ab) or control IgG (DIO + IgG). The same mice were used in **b**–**e**. High-fat diet was started at the age of 4-weeks-old, and all of the mice were examined at 12-weeks-old. ($n = 5$ mice in each group). (**b**) Histochemical identification of endothelial cells (lectin, red), adipocytes (BODIPY, blue) and nuclei (Hoechst, green) in epididymal adipose tissue. White arrows indicate CLSs. Scale bars, 100 μm. (**c**) Real-time PCR analysis of cytokine expression in adipose tissue. The levels of each transcript were normalized to that in the lean control ($n = 5$ mice in each group). AU, arbitrary units. (**d**,**e**) Results of insulin tolerance (**d**, 0.75 U insulin per kg body weight) and oral glucose tolerance (**e**, 1 g per kg glucose) tests in DIO mice treated with antibody to CD8 or control IgG ($n = 8$ mice in each group). $^*P < 0.05$. Error bars represent means ± s.e.m.

It is known that one consequence of macrophage accumulation, particularly M1 macrophages, in inflamed adipose tissue is modulation and impairment of the tissue's function[17]. It is not known, however, what initiates macrophage infiltration or the resultant inflammatory cascade. The dynamic changes in lymphocyte populations seen in obese adipose tissue (**Fig. 1a,b**) suggest that lymphocytes might have a key role. To test this idea, we examined the time course of changes in stromal cell populations during the progression of DIO. We fed C57BL/6 mice a high-fat diet, beginning when they were 4-weeks-old (**Fig. 1d–g**). Within 2 weeks, the $CD8^+CD4^-$ T cell fraction within the total stromal vascular cell fraction was significantly increased in the stroma of the epididymal fat, as compared to that in mice fed a control chow diet (**Fig. 1e**). The numbers of $CD8^+CD4^-$ T cells continued to increase thereafter, peaking when the mice were 15-weeks-old (**Fig. 1e**). By contrast, the fractions of $CD8^-CD4^+$ T cells and $CD4^+CD25^+FoxP3^+$ regulatory T cells were reduced at later times (**Fig. 1f,g**), suggesting that $CD8^+$ T cell infiltration is a primary event during inflammatory cascades within adipose tissue. The increase in $CD8^+$ T cells also preceded the accumulation of macrophages when cell numbers were expressed per fat pad (**Supplementary Fig. 5**), clearly indicating that $CD8^+$ cells infiltrated into the epididymal fat pads of DIO mice before macrophage infiltration.

To gain additional insight into the clinical importance of $CD8^+$ T cells in obese fat, we analyzed the expression of *CD8A* in samples of human subcutaneous adipose tissue. Levels of *CD8A* expression were significantly higher in obese subjects than in lean ones ($P < 0.05$), suggesting that $CD8^+$ T cells also accumulate in human obese adipose tissue (**Supplementary Fig. 6**).

CD8 depletion inhibits inflammatory cascade in obese adipose

To assess the role of $CD8^+$ T cells in adipose inflammation, we examined the effects of CD8 depletion using neutralizing antibody treatment on the inflammatory response in obese adipose tissue. We randomly assigned male C57BL/6 mice to two groups and intraperitoneally administered either antibody to CD8 or control IgG once a week for 8 weeks, beginning when the mice were 4-weeks-old. We fed the mice a high-fat diet over the same period, and we performed metabolic and histological analyses at 12 weeks of age. Antibody to CD8 treatment had no effect on body weight, food intake, fat pad weight or adipocyte diameter (**Supplementary Fig. 7**). However, it significantly lowered the $CD8^+CD4^-$ T cell fraction in the epididymal fat pads without affecting the $CD8^-CD4^+$ cell fraction (**Fig. 2a**). It also reduced the infiltrated M1 macrophage ($F4/80^+CD11c^+CD206^-$) fraction without affecting the M2 macrophage ($F4/80^+CD11c^-CD206^+$) fraction[17] and significantly lowered the numbers of CLSs ($P < 0.05$ for each) (**Fig. 2b** and **Supplementary Fig. 7d**).

The messenger RNA expression of the proinflammatory cytokines interleukin-6 (IL-6) and tumor necrosis factor-α (TNF-α) in epididymal fat pads was lowered by CD8-specific antibody treatment (**Fig. 2c**), as were their serum concentrations (**Supplementary Fig. 7f**). In addition, the insulin resistance and glucose intolerance induced by the high-fat diet were ameliorated by CD8-specific antibody treatment (**Fig. 2d,e**). Similarly, CD8-specific antibody treatment lowered M1 macrophage infiltration into epididymal fat and ameliorated systemic insulin resistance in *ob/ob* mice (**Supplementary Fig. 8**). Collectively, these effects of CD8-specific antibody treatment clearly show that $CD8^+$ cells are required for the recruitment of macrophages into obese adipose tissue and the initiation and propagation of inflammatory responses there.

CD8 depletion ameliorates pre-established inflammation

We next examined the activity of $CD8^+$ T cells in obese adipose tissues in which inflammation had already been established. We began administering antibodies to 19-week-old DIO mice that had been fed a high-fat diet since they were 9-weeks-old. We intraperitoneally administered either antibody to CD8 or control IgG three times per week for 2 weeks, and examined the mice at 21-weeks-old. Treatment with antibody to CD8 suppressed $CD8^+$ T cell infiltration into obese fat pads without affecting $CD4^+$ T cells (**Fig. 3a**). CD8 antibody also lowered M1 ($F4/80^+CD11c^+$) macrophage fraction while leaving the M2 macrophage ($F4/80^+CD11c^-$) fraction unchanged (**Fig. 3a**). The reduction in macrophage infiltration was confirmed by F4/80 immunohistochemistry (**Fig. 3b**). In addition, the number of CLSs was also lowered by CD8-specific antibody treatment (**Fig. 3b,c**). DIO led to upregulated mRNA expression of the proinflammatory cytokines IL-1, IL-6 and TNF-α, as well as of

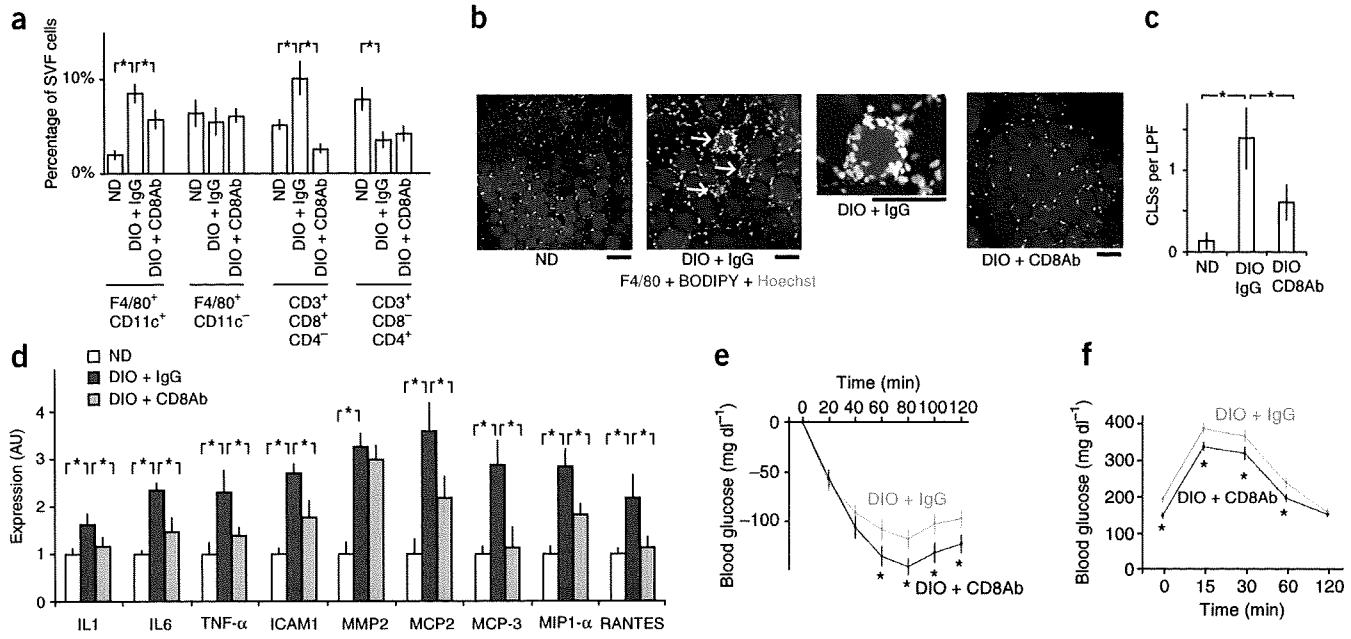

Figure 3 Effects of CD8-specific antibody treatment on pre-established obese adipose inflammation. (**a**) Flow cytometric analysis of cell populations in stromal vascular fractions from control mice on a normal chow diet (ND) and DIO mice administered control IgG (DIO + IgG) or antibody to CD8 (DIO + CD8Ab) three times per week from 19- to 21-weeks-old. ($n = 5$ mice in each group). High-fat diet was started at the age of 9-weeks-old, and all the mice were examined at 21-weeks-old. The same mice were used in **b–f**. (**b**) Immunohistochemical identification of macrophages (F4/80, red) in epididymal adipose tissue. Adipocytes were counterstained with BODIPY (blue), and the nuclei with Hoechst (green). Scale bars, 100 μm. (**c**) Numbers of CLSs (shown by white arrows in **b**) in adipose tissue ($n = 20$ low-power fields (LPF) in each group). (**d**) Real-time PCR analysis of cytokine expression in epididymal adipose tissue. The levels of each transcript were normalized to those in control ND mice. MIP, monocyte inflammatory protein ($n = 5$ mice in each group). (**e,f**) Results of insulin tolerance (**e**, 1 U insulin per kg body weight) and oral glucose tolerance (**f**, 1 g per kg glucose) tests in DIO mice treated with antibody to CD8 or control IgG ($n = 10$ mice in each group). $^*P < 0.05$. Error bars represent means ± s.e.m.

intercellular adhesion molecule-1 (ICAM1) and matrix metalloproteinase-2 (MMP-2), in adipose tissue, which is consistent with local inflammation, and CD8-specific antibody treatment lowered expression of all of these mediators (**Fig. 3d**).

CD8-specific antibody treatment also ameliorated insulin resistance and glucose intolerance in DIO mice (**Fig. 3e,f** and **Supplementary Fig. 9**). These results clearly show that CD8-specific antibody treatment suppresses preexisting adipose inflammation, which strongly suggests that $CD8^+$ cells are required for the maintenance of inflammatory reactions in obese adipose tissue.

$CD8^+$ T cells are required for adipose tissue inflammation

To further establish the requirement for $CD8^+$ T cells in adipose inflammation *in vivo*, we started 6-week-old genetically CD8-deficient mice on a high-fat diet and maintained them on it for 8 weeks, and examined the $CD8a^{-/-}$ mice at 14-weeks-old. In sharp contrast to wild-type mice fed the same high-fat diet (**Fig. 1**), the CD8-deficient mice did not show significant increases in the M1 or M2 macrophage fraction in the epididymal fat under high-fat diet (**Fig. 4a**), and we found very few CLSs (**Fig. 4b,c**), although both body weight and epididymal fat mass were significantly higher compared to $CD8a^{-/-}$ mice on a normal diet (**Supplementary Fig. 10a,b**). Levels of proinflammatory cytokine mRNA expression in adipose tissue, including IL-6 and TNF-α, also were not increased by the high-fat diet in CD8-deficient mice (**Fig. 4d**).

To directly examine the role of $CD8^+$ T cells in adipose tissue inflammation, we adoptively transferred splenic $CD8^+$ T cells into CD8-deficient mice. We intravenously administered either 5×10^6 splenic $CD8^+$ T cells isolated from 7-week-old C57BL/6 mice or control vehicle weekly over the same period and examined the $CD8a^{-/-}$ mice at 14-weeks-old. Adoptive transfer of $CD8^+$ T cells increased M1 macrophage infiltration (**Fig. 4a**), numbers of CLSs (**Fig. 4b,c**), and expression of IL-6 and TNF-α in epididymal fat (**Fig. 4d**), indicating initiation of adipose inflammation. A high-fat diet induced moderate glucose intolerance in untreated CD8-deficient mice, but we did not observe insulin resistance in insulin tolerance tests (**Fig. 4e,f**). Adoptive $CD8^+$ T cell transfer aggravated the glucose intolerance and induced insulin resistance (**Fig. 4e,f**). Taken together, the results that we obtained with CD8-deficient mice confirm that $CD8^+$ T cells are essential for macrophage recruitment and inflammation in adipose tissue in DIO.

Interplay between macrophages, T cells and adipocytes

We next analyzed the cellular interplay via which inflammation develops in obese adipose tissue. On the basis of the findings of the *in vivo* experiments summarized above, we hypothesized that obese adipose tissue activates $CD8^+$ T cells, which, in turn, recruit and activate macrophages. To test this hypothesis, we first cocultured splenic $CD8^+$ T cells with epididymal fat tissue prepared from lean or obese mice to determine whether obese adipose tissue can activate $CD8^+$ T cells. Whereas obese epididymal fat clearly induced T cell proliferation, lean fat did so only modestly (**Fig. 5a**), indicating that obese adipose tissue can indeed activate $CD8^+$ T cells.

To assess the involvement of $CD8^+$ T cells in monocytes and macrophage differentiation, we cocultured various combinations of peripheral blood $CD11b^{high}$ granulocyte-1 $(Gr\text{-}1)^-CD4^-CD8^-$cells (most of which were monocytes), $CD8^+$ cells prepared from either lean or obese adipose tissue, and lean epididymal adipose tissue. By

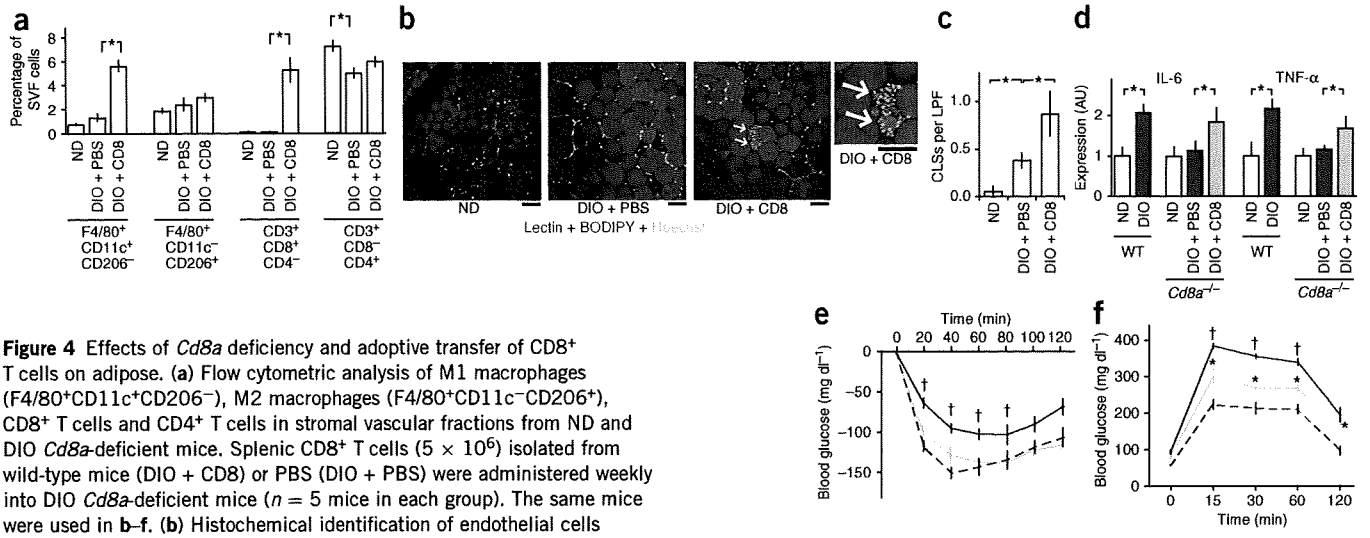

Figure 4 Effects of *Cd8a* deficiency and adoptive transfer of CD8+ T cells on adipose. (**a**) Flow cytometric analysis of M1 macrophages (F4/80+CD11c+CD206−), M2 macrophages (F4/80+CD11c−CD206+), CD8+ T cells and CD4+ T cells in stromal vascular fractions from ND and DIO *Cd8a*-deficient mice. Splenic CD8+ T cells (5×10^6) isolated from wild-type mice (DIO + CD8) or PBS (DIO + PBS) were administered weekly into DIO *Cd8a*-deficient mice ($n = 5$ mice in each group). The same mice were used in **b**–**f**. (**b**) Histochemical identification of endothelial cells (lectin, red), adipocytes (BODIPY, blue) and nuclei (Hoechst, green) in epididymal adipose tissue. White arrows indicate CLSs. Scale bars, 100 μm. (**c**) Numbers of CLSs in adipose tissues ($n = 20$ low-power fields in each group). (**d**) Real-time PCR analysis of cytokine expression in adipose tissue from C57BL/6 (WT) ND, WT DIO, and *Cd8a*-deficient ND, DIO + CD8 or DIO + PBS mice. ($n = 5$ mice in each group). $^*P < 0.05$ in **a**–**d**. (**e**,**f**) Insulin tolerance (**e**, 0.75 U insulin per kg body weight) and oral glucose tolerance (**f**, 1 g per kg) tests of the *Cd8a*-deficient ND (dotted lines), DIO + CD8 and DIO + PBS groups ($n = 6$ mice in each group). $^*P < 0.05$ for ND versus DIO + PBS and $\dagger P < 0.05$ for DIO + PBS versus DIO + CD8. Error bars represent means ± s.e.m.

themselves, neither CD8+ cells nor adipose tissue induced macrophage differentiation (**Fig. 5b**). However, when cocultured with both CD8+ cells and lean adipose tissue, peripheral blood monocytes differentiated into F4/80+CD11b+CD68+ macrophages (**Fig. 5b**). Moreover, CD8+ cells from obese adipose tissues generated significantly more macrophages than those from lean adipose (**Fig. 5b**). Thus, CD8+ cells seem to be essential for macrophage differentiation in this setting. Further, the requirement for adipose tissue suggests that the interaction between CD8+ T cells and adipose tissue is necessary for induction of macrophage differentiation.

We then tested whether activated CD8+ cells elicit macrophage migration via humoral interactions. Analysis of the medium conditioned with activated CD8+ T cells showed that these cells secrete substantial amounts of humoral factors known to induce macrophage

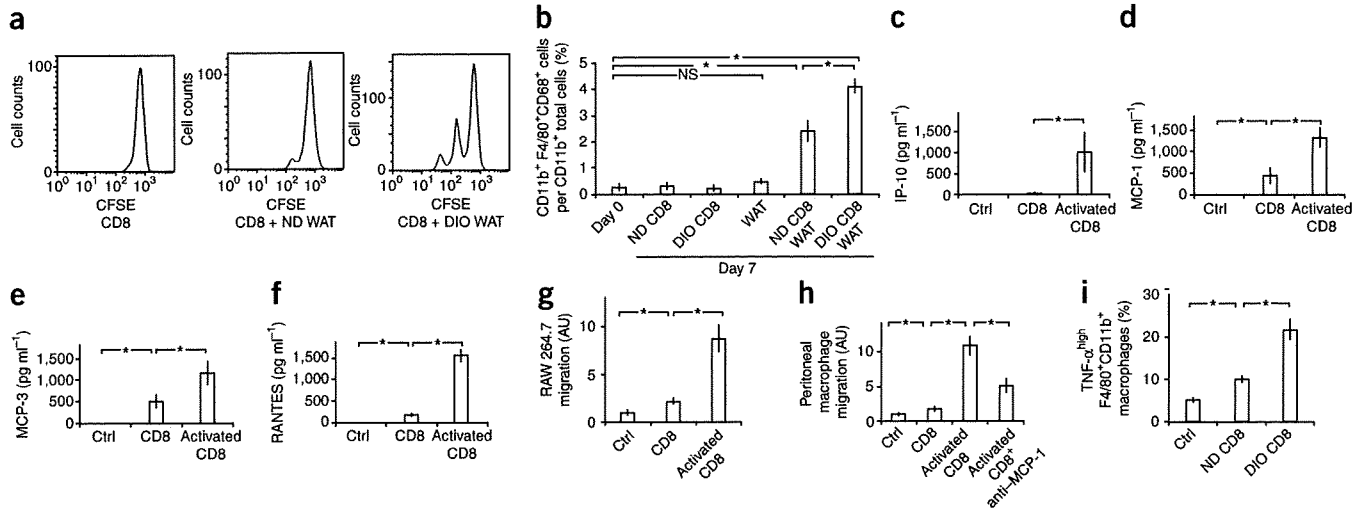

Figure 5 Interplay between macrophages, CD8+ T cells and adipose tissue. (**a**) Carboxyfluorescein succinimidyl ester (CFSE) proliferation assay of isolated splenic CD8+ T cells cultured with or without epididymal adipose tissue from ND or DIO mice. WAT, white adipose tissue. (**b**) Effects of CD8+ T cells and adipose tissue on differentiation of peripheral blood monocytes ($CD11b^{high}Gr\text{-}1^-$) into macrophages (CD11b+F4/80+CD68+). Monocytes were cocultured for 7 d with CD8+ T cells isolated from epididymal adipose tissue from lean (ND CD8) or DIO (DIO CD8) mice, with or without epididymal WAT from lean mice. The differentiated macrophage fractions are shown ($n = 5$ in each group; $^*P < 0.05$; NS, not significant). (**c**–**f**) Concentrations of various cytokines in the control medium and medium conditioned by quiescent (CD8) or activated (activated CD8) CD8 cells ($n = 5$ in each group). $^*P < 0.05$. IP-10, interferon-inducible protein-10. (**g**,**h**) Migration of RAW264.7 (**g**) and peritoneal (**h**) macrophages, as examined using unconditioned control medium (Ctrl), medium conditioned by quiescent (CD8) or activated (activated CD8) CD8+ T cells, or neutralizing antibody to MCP-1 (anti–MCP-1) ($n = 20$ in each group). $^*P < 0.05$. (**i**) The fraction of F4/80+ CD11b+ macrophages producing high levels of TNF-α after isolation from lean epididymal adipose tissue and cultured without (Ctrl) or with CD8+ T cells isolated from ND (ND CD8) or DIO (DIO CD8) mice ($n = 5$ in each group, $^*P < 0.05$). Error bars represent means ± s.e.m.

migration, including interferon-inducible protein-10, monocyte chemoattractant protein-1 (MCP-1), MCP-3 and regulation upon activation, normal T cell expressed and secreted protein (RANTES) (**Fig. 5c–f**). When we plated cells of the macrophage cell line RAW264.7 or isolated peritoneal macrophages in Boyden chambers and treated them with medium conditioned by activated $CD8^+$ T cells, the numbers of both cell types that migrated through the pores between the chamber wells with activated $CD8^+$ T cell–conditioned medium were significantly higher compared to cells cultured in non-conditioned medium ($P < 0.05$ for each) (**Fig. 5g,h**). Treatment with antibody to MCP-1 lowered the migration of peritoneal macrophages by approximately half, indicating MCP-1 to be one of the factors mediating the humoral interactions (**Fig. 5h**).

To further assess the involvement of $CD8^+$ T cells in macrophage activation in adipose tissue, we cocultured $F4/80^+$ $CD11b^+$ macrophages isolated from lean epididymal fat tissue with $CD8^+$ cells isolated from either lean or obese fat tissue. The numbers of macrophages producing high amounts of TNF-α were significantly increased by the $CD8^+$ cells (**Fig. 5i**). Moreover, $CD8^+$ cells from obese adipose tissue increased the number of TNF-α^{high} macrophages to a significantly greater degree than those from lean adipose tissue (**Fig. 5i**). Collectively, then, the results of the coculture experiments show that the interaction between obese adipose tissue and $CD8^+$ T cells is crucial for macrophage differentiation, migration and activation.

DISCUSSION

Adipose tissue inflammation is now considered to be a crucial event leading to the metabolic syndrome, diabetes and atherosclerotic cardiovascular disease. However, it is still unclear how adipose inflammation is initiated and maintained. Here we showed that $CD8^+$ T cell infiltration precedes accumulation of macrophages in adipose tissue obesity, $CD8^+$ T cells are required for adipose tissue inflammation and $CD8^+$ T cells have major roles in macrophage differentiation, activation and migration. Thus, $CD8^+$ T cells are crucially involved in initiating inflammatory cascades in obese adipose tissue. Moreover, the finding that CD8-specific antibody treatment ameliorates preestablished adipose inflammation in DIO mice indicates that $CD8^+$ T cells are also essential for maintenance of the inflammatory response. Although infiltration of T cells into obese adipose tissue has been reported previously[10,18], to our knowledge, the present study is the first to directly address the functional role of $CD8^+$ cells in adipose tissue inflammation. The findings that systemic insulin resistance is ameliorated by CD8 depletion and aggravated by adoptive transfer of $CD8^+$ cells strongly suggest that CD8-dependent adipose inflammation has an impact on systemic metabolism.

Accumulation of $CD8^+$ T cells in obese epididymal fat pads was not accompanied by the presence of greater numbers of $CD8^+$ T cells in the systemic circulation, suggesting that $CD8^+$ T cells are activated by endogenous stimuli localized in the adipose tissue. Supporting this notion is our finding that obese adipose tissue induces $CD8^+$ T cell proliferation. The findings that incubation with $CD8^+$ T cells plus lean adipose tissue induced macrophage differentiation, although neither $CD8^+$ T cells nor lean adipose tissue did so alone, suggest that $CD8^+$ T cells and adipose tissue interact with each other to activate a local inflammatory cascade. In addition, the results of coculture experiments showing the interactions among $CD8^+$ T cells, macrophages and adipose tissue, as well as the results of our CD8 depletion experiments, which showed that $CD8^+$ T cells are essential for both the initiation and maintenance of adipose inflammation, strongly suggest that there is a relay involving both $CD8^+$ T cells and macrophages in obese adipose tissue that propagates local adipose inflammation.

In contrast to the increased infiltration of $CD8^+$ T cells, numbers of $CD4^+$ T cells and regulatory T cells were low at later time points (**Fig. 1**), which would also be expected to contribute to local inflammation within adipose tissue. For instance, subsets of $CD4^+$ T cells are known to secrete cytokines that can inhibit macrophage recruitment, including IL-4 and IL-10 (ref. 19), whereas regulatory T cells control adaptive immune responses by suppressing T cells, NK cells, NKT cells, B cells and dendritic cells[20]. In addition, regulatory T cells have also been shown to inhibit proinflammatory activation of monocytes[21] and to inhibit macrophage infiltration and renal injury in a model of chronic kidney disease[22]. It is therefore tempting to speculate that reducing the numbers of $CD4^+$ and regulatory T cells augments the inflammatory response during the late phase of adipose tissue obesity.

Taken together, our results support the idea that obese adipose tissue activates $CD8^+$ T cells, which, in turn, initiate and propagate inflammatory cascades, including the recruitment of monocytes and macrophages into obese adipose tissues and their subsequent differentiation and activation there. Thus, it seems that $CD8^+$ T cells have a primary role in obese adipose tissue inflammation, though future studies are needed to address which environmental cues within obese adipose tissue initiate $CD8^+$ cell infiltration. Even so, these results further support the idea that adipose inflammation has a major impact on systemic metabolism.

METHODS

Methods and any associated references are available in the online version of the paper at http://www.nature.com/naturemedicine/.

Note: Supplementary information is available on the Nature Medicine website.

ACKNOWLEDGMENTS

We gratefully acknowledge A. Matsuoka, X. Yingda, E. Magoshi, M. Hayashi, K. Wakabayashi, M. Tajima and Y. Yamazaki for excellent technical assistance. This study was supported by Research Fellowships from the Japan Society for the Promotion of Science for Young Scientists (S.N.), Grants-in-Aid for Scientific Research (I.M., R.N.) and grants for Translational Systems Biology and Medicine Initiative (R.N., T.K.) and Global Centers of Excellence program (R.N., T.K.) from the Ministry of Education, Culture, Sports, Science and Technology of Japan and a research grant from the National Institute of Biomedical Innovation (R.N.).

AUTHOR CONTRIBUTIONS

S.N. and M.N. performed *in vivo* and *in vitro* assays and analyzed all of the end points. K.H., K.U. and K.Y. performed human subject assays. S.N., I.M., K.E., H.Y., M. Otsu, M. Ohsugi, S.S., T.K. and R.N. supervised entire studies. S.N. and I.M. wrote the manuscript.

Published online at http://www.nature.com/naturemedicine/.
Reprints and permissions information is available online at http://npg.nature.com/reprintsandpermissions/.

1. Hotamisligil, G.S. Inflammation and metabolic disorders. *Nature* **444**, 860–867 (2006).
2. Weisberg, S.P. *et al.* Obesity is associated with macrophage accumulation in adipose tissue. *J. Clin. Invest.* **112**, 1796–1808 (2003).
3. Nishimura, S. *et al. In vivo* imaging in mice reveals local cell dynamics and inflammation in obese adipose tissue. *J. Clin. Invest.* **118**, 710–721 (2008).
4. Xu, H. *et al.* Chronic inflammation in fat plays a crucial role in the development of obesity-related insulin resistance. *J. Clin. Invest.* **112**, 1821–1830 (2003).
5. Savage, D.B., Petersen, K.F. & Shulman, G.I. Disordered lipid metabolism and the pathogenesis of insulin resistance. *Physiol. Rev.* **87**, 507–520 (2007).
6. Guilherme, A., Virbasius, J.V., Puri, V. & Czech, M.P. Adipocyte dysfunctions linking obesity to insulin resistance and type 2 diabetes. *Nat. Rev. Mol. Cell Biol.* **9**, 367–377 (2008).
7. Shoelson, S.E., Lee, J. & Goldfine, A.B. Inflammation and insulin resistance. *J. Clin. Invest.* **116**, 1793–1801 (2006).
8. Suganami, T., Nishida, J. & Ogawa, Y. A paracrine loop between adipocytes and macrophages aggravates inflammatory changes: role of free fatty acids and tumor necrosis factor alpha. *Arterioscler. Thromb. Vasc. Biol.* **25**, 2062–2068 (2005).

9. Wu, H. *et al.* T-cell accumulation and regulated on activation, normal T cell expressed and secreted upregulation in adipose tissue in obesity. *Circulation* **115**, 1029–1038 (2007).
10. Rausch, M.E., Weisberg, S., Vardhana, P. & Tortoriello, D.V. Obesity in C57BL/6J mice is characterized by adipose tissue hypoxia and cytotoxic T-cell infiltration. *Int. J. Obes. (Lond.)* **32**, 451–463 (2008).
11. Monney, L. *et al.* T_H1-specific cell surface protein Tim-3 regulates macrophage activation and severity of an autoimmune disease. *Nature* **415**, 536–541 (2002).
12. Brake, D.K., Smith, E.O., Mersmann, H., Smith, C.W. & Robker, R.L. ICAM-1 expression in adipose tissue: effects of diet-induced obesity in mice. *Am. J. Physiol. Cell Physiol.* **291**, C1232–C1239 (2006).
13. Traktuev, D.O. *et al.* A population of multipotent CD34-positive adipose stromal cells share pericyte and mesenchymal surface markers, reside in a periendothelial location and stabilize endothelial networks. *Circ. Res.* **102**, 77–85 (2008).
14. Nishimura, S. *et al.* Adipogenesis in obesity requires close interplay between differentiating adipocytes, stromal cells and blood vessels. *Diabetes* **56**, 1517–1526 (2007).
15. Cinti, S. *et al.* Adipocyte death defines macrophage localization and function in adipose tissue of obese mice and humans. *J. Lipid Res.* **46**, 2347–2355 (2005).
16. Sallusto, F., Lenig, D., Forster, R., Lipp, M. & Lanzavecchia, A. Two subsets of memory T lymphocytes with distinct homing potentials and effector functions. *Nature* **401**, 708–712 (1999).
17. Lumeng, C.N., Bodzin, J.L. & Saltiel, A.R. Obesity induces a phenotypic switch in adipose tissue macrophage polarization. *J. Clin. Invest.* **117**, 175–184 (2007).
18. Kintscher, U. *et al.* T-lymphocyte infiltration in visceral adipose tissue: a primary event in adipose tissue inflammation and the development of obesity-mediated insulin resistance. *Arterioscler. Thromb. Vasc. Biol.* **28**, 1304–1310 (2008).
19. Miller, R., Wen, X., Dunford, B., Wang, X. & Suzuki, Y. Cytokine production of $CD8^+$ immune T cells but not of $CD4^+$ T cells from *Toxoplasma gondii*–infected mice is polarized to a type 1 response following stimulation with tachyzoite-infected macrophages. *J. Interferon Cytokine Res.* **26**, 787–792 (2006).
20. Sakaguchi, S. *et al.* $Foxp3^+$ $CD25^+$ $CD4^+$ natural regulatory T cells in dominant self-tolerance and autoimmune disease. *Immunol. Rev.* **212**, 8–27 (2006).
21. Taams, L.S. *et al.* Modulation of monocyte/macrophage function by human $CD4^+CD25^+$ regulatory T cells. *Hum. Immunol.* **66**, 222–230 (2005).
22. Mahajan, D. *et al.* $CD4^+CD25^+$ regulatory T cells protect against injury in an innate murine model of chronic kidney disease. *J. Am. Soc. Nephrol.* **17**, 2731–2741 (2006).

ONLINE METHODS

Mice. We obtained Male C57BL/6J, *ob/ob* and *Cd8a*-deficient mice from Charles River Japan or Jackson Laboratories. All mice were housed under a 12-h light-dark cycle and allowed free access to food. To examine the time-course of changes in stromal vascular cell populations in adipose tissue under conditions of diet-induced obesity, we divided C57BL/6 mice into two groups and fed either a standard chow diet (6% fat, Oriental Yeast Company) or a high-fat diet (D12492, 60 Kcal% fat, Research Diets) from the age of 4 weeks.

To examine the effects of CD8 depletion on the initiation and development of adipose inflammation, we started antibody administration before the establishment of DIO. We fed male C57BL/6 mice a high-fat diet for 8 weeks, beginning when they were 4-weeks-old, and we intraperitoneally administered either CD8-specific antibody (3 μg per g body weight, 1 mg ml^{-1} solution, Biolegend) or control rat IgG (Sigma, 1 mg ml^{-1} PBS solution) weekly over the same period. We examined the mice at 12 weeks old (**Fig. 2** and **Supplementary Fig. 7**). We validated depletion of $CD8^+$ T cells by antibody as shown in **Supplementary Figure 11**.

To assess the effects of CD8 depletion on preestablished adipose inflammation in DIO mice, we fed C57BL/6 mice a high-fat diet, beginning when they were 9-weeks-old. Ten weeks later, we randomly assigned the 19-week-old obese mice to two groups and we intraperitoneally administered either CD8-specific antibody (120 μg per mouse) or control IgG three times per week for 2 weeks (total of six administrations). Age-matched lean C57BL/6 mice fed a normal chow diet served as controls. At 21 weeks, we performed oral glucose and insulin tolerance tests and then killed the mice for analysis of their adipose tissue (**Fig. 3** and **Supplementary Fig. 9**).

To assess the effects of CD8-deficient and adoptive transfer of $CD8^+$ T cells on adipose inflammation, we fed *CD8a*$^{-/-}$ mice either normal chow or a high-fat diet for 8 weeks, beginning when they were 6-weeks-old. We intravenously administered either 5×10^6 splenic $CD8^+$ T cells or control PBS weekly over the same period. We examined the *CD8a*$^{-/-}$ mice at 14-weeks-old. We prepared $CD8^+$ splenic T cells from 7-week-old C57BL/6 mice (**Fig. 4** and **Supplementary Fig. 10**). All experiments were approved by the Institutional Committee for Animal Research of The University of Tokyo and strictly adhered to the guidelines for animal experiments of The University of Tokyo.

Isolation of the stromal vascular fraction and flow cytometry. We isolated stromal vascular cells using previously described methods with some modifications. We killed the mice after general anesthesia after systemic heparinization. We removed the epididymal and subcutaneous adipose tissues and then minced it into small pieces (~2 mm). We vigorously agitated the pieces in PBS supplemented with 1 μg ml^{-1} heparin for 30 s to remove any circulating blood cells and then centrifuged the suspension at 1,000*g* for 8 min. We collected floating pieces of adipose tissue and incubated them for 20 min in collagenase solution (2 mg ml^{-1} of collagenase type 2 (Worthington) in Tyrode buffer (containing 137 mM NaCl, 5.4 mM KCl, 1.8 mM $CaCl_2$, 0.5 mM $MgCl_2$, 0.33 mM NaH_2PO_4, 5 mM HEPES and 5 mM glucose)) with gentle stirring. We then centrifuged the digested tissue again at 1,000*g* for 8 min. We resuspended the resultant pellet containing the stromal vascular fraction into PBS and filtered it through a 70-μm mesh. We washed the cells twice with PBS, incubated for 10 min in erythrocyte-lysing buffer (Becton Dickinson) as previously described[3], and we finally resuspended them in PBS supplemented with 3% FBS. We incubated these isolated cells with either labeled monoclonal antibody or isotype control antibody (eBioscience and BD Pharmingen) and analyzed by flow cytometry with a Vantage flow cytometer (Becton Dickinson) and FlowJo (Tree Star, Inc.) software. We used propidium iodide (Invitrogen) to exclude dead cells. We validated flow cytometric identification of M1 ($F4/80^+CD11c^+$) and M2 ($F4/80^+CD11c^-$) macrophages with CD11c markers as described in the **Supplementary Methods** and **Supplementary Figure 12**.

Immunohistochemistry. We stained and visualized whole-mount adipose tissue as previously described[14].

CFSE proliferation assay of $CD8^+$ T cells. We isolated splenic $CD8^+$ T cells from 7-week-old C57BL/6 mice and incubated the isolated $CD3^+$ $CD8^+$ cells with 5 μM CFSE (CellTrace CFSE Cell Proliferation Kit, Invitrogen). After staining, we incubated 2×10^5 cells in DMEM supplemented with 3% FBS for 2 d, with or without 20 mg of minced epididymal white adipose tissue prepared from either 20-week-old lean mice fed a normal chow diet or DIO mice fed a high-fat diet for 16 weeks. We harvested the $CD8^+$ cells and then analyzed them by flow cytometry to examine the proliferation status.

Differentiation of peripheral blood monocytes into macrophages. We isolated peripheral blood monocytes ($CD11b^{high}Gr\text{-}1^-$) from lean 7-week-old C57BL/6 mice. In the lower wells of a 24-well Multiwell Boyden chamber (Becton Dickinson), we cultured 5×10^4 monocytes per well in DMEM supplemented with 3% FBS, with or without 10 mg of minced epididymal adipose tissue prepared from 7-week-old lean mice in the upper wells. Also in the upper wells, we cultured 5×10^4 $CD3^+CD8^+CD4^-$ T cells, which we isolated from epididymal adipose tissues of 20-week-old lean or DIO mice. We incubated the cells for 7 d, after which the cells in the upper wells were collected, stained for CD11b, F4/80 and CD68, and assayed by flow cytometry for the differentiated macrophage fractions ($CD11b^+F4/80^+CD68^+$).

Migration of RAW264.7 and peritoneal macrophages. We isolated $CD8^+$ T cells from blood collected from C57BL/B6J mice after cardiac puncture. We isolated and cultured $CD3^+CD8^+$ cells were in DMEM supplemented with 3% FBS. To activate $CD8^+$ T cells, we cultured the cells with recombinant IL-2 (20 U ml^{-1}; Sigma), Dynabeads CD3/CD28 T Cell Expander (a bead-to-cell ratio of 1:1) and 2-mercaptoethanol (50 μM). After 120 h of culture, we aspirated the culture medium and performed migration assay using Boyden chambers with 8-μm pore inserts (Becton Dickinson). We cultured RAW264.7 and peritoneal macrophages in the upper wells, and we added the conditioned medium to the lower wells. We used fresh DMEM supplemented with 5% FBS as a control. To inhibit MCP-1 activity, we added a neutralizing antibody (5 μg ml^{-1} antibody to MCP-1, clone 2H5, Biolegend) to the conditioned medium.

TNF-α production in macrophages cocultured with $CD8^+$ cells. We isolated $F4/80^+$ $CD11b^+$ macrophages from epididymal adipose tissue from lean 7-week-old C57Bl/B6J mice, and we isolated $CD3^+CD8^+CD4^-$ T cells from epididymal adipose tissue from 20-week-old lean or DIO mice. We then added the adipose macrophages to the upper wells of a Multiwell Boyden chamber (Becton Dickinson) (5×10^4 cells per well), and we added the same number of $CD8^+$ T cells to the lower wells, after which we cultured the cells in DMEM supplemented with 3% FBS for 7 d. We assessed intracellular production of TNF-α by flow cytometry using an intracellular cytokine production detection kit (Cytofix/Cytoperm Fixation/Permeabilization Solution Kit, BD Pharmingen).

Human subjects. We acquired subcutaneous adipose tissue from healthy female donors undergoing liposuction of the abdomen or thighs (after obtaining their consent). We examined expression of *CD8a* in the tissue. We processed samples comprised of 1 g of each specimen by digestion with collagenase and then centrifuged to isolate the stromal vascular fractions. We purified total RNA using Trizol (Invitrogen) and determined relative mRNA levels using real-time PCR. This study was approved by the Ethics Committee of The University of Tokyo Hospital.

Statistical analyses. We expressed the results as means ± s.e.m. We determined the statistical significance of differences between two groups using Student's *t* tests, and we evaluated differences among three groups by analysis of variance followed by *post-hoc* Bonferroni tests. Values of $P < 0.05$ were considered significant.

THE JOURNAL OF BIOLOGICAL CHEMISTRY VOL. 284, NO. 45, pp. 31463–31472, November 6, 2009

Evidence That Integrin αIIbβ3-dependent Interaction of Mast Cells with Fibrinogen Exacerbates Chronic Inflammation*

Received for publication, June 6, 2009, and in revised form, July 22, 2009 Published, JBC Papers in Press, September 15, 2009, DOI 10.1074/jbc.M109.030213

Toshihiko Oki[‡], Koji Eto[§], Kumi Izawa[‡], Yoshinori Yamanishi[‡], Naoki Inagaki[¶], Jon Frampton[‖], Toshio Kitamura[‡], and Jiro Kitaura[‡1]

From the [‡]Division of Cellular Therapy, Advanced Clinical Research Center, The Institute of Medical Science, The University of Tokyo, 4-6-1 Shirokanedai, Minato-ku, Tokyo 108-8639, Japan, the [§]Division of Stem Cell Therapy, Center for Stem Cell and Regenerative Medicine, The Institute of Medical Science, University of Tokyo, Tokyo 108-8639, Japan, the [¶]Department of Pharmacology, Gifu Pharmaceutical University, Gifu 502-8585, Japan, and the [‖]Division of Immunity and Infection, Medical Research Council Centre for Immune Regulation, University of Birmingham, Birmingham B15 2TT, United Kingdom

Integrin αIIbβ3 is expressed in mast cells as well as in megakaryocytes/platelets. A recent study has shown that surface expression levels of integrin αVβ3 are elevated in integrin αIIb-deficient bone marrow-derived mast cells (BMMCs) as compared with wild-type (WT) counterparts, but the underlying mechanism remains obscure. Here we demonstrate by transducing integrin αIIb into integrin αIIb-deficient BMMCs that surface expression levels of integrin αVβ3 are inversely related to those of integrin αIIbβ3. Thus, competitive association of integrin β3 with integrin αIIb or integrin αV determines surface expression levels of integrin αIIbβ3 or αVβ3 in mast cells. We compared WT and integrin αIIb-deficient BMMCs as well as integrin αIIb-deficient BMMCs transduced with integrin αIIb(WT) or non-functional αIIb(D163A) mutant and found that enhancement of proliferation, degranulation, cytokine production, and migration of BMMCs through interaction with fibrinogen (FB) depended on integrin αIIbβ3. In addition, elevated surface expression of integrin αVβ3 failed to compensate for loss of FB-associated functions in integrin αIIb-deficient BMMCs while enhancing adhesion to vitronectin or von Willebrand factor. Importantly, integrin αIIb deficiency strongly suppressed chronic inflammation with the remarkable increase of mast cells induced by continuous intraperitoneal administration of FB, although it did not affect acute allergic responses or mast cell numbers in tissues in steady states. Interestingly, soluble FB promoted cytokine production of BMMCs in response to *Staphylococcus aureus* with FB-binding capacity, through integrin αIIbβ3-dependent recognition of this pathogen. Collectively, integrin αIIbβ3 in mast cells plays an important part in FB-associated, chronic inflammation and innate immune responses.

Mast cells play a critical role in IgE-associated allergic disorders, but recent advances have delineated the involvement of mast cells in IgE-independent physiological and pathological processes, including certain innate immune responses. In fact, various stimuli, in addition to IgE and specific antigens, can activate mast cells to release a diverse array of preformed and newly synthesized pro-inflammatory mediators such as histamine, lipids, cytokines, and chemokines (1–4). Although mast cell numbers and activation in tissues are closely related to mast cell-mediated immunity, the underlying mechanism remains incompletely understood. As one of the key phenomena, mast cells interact with the extracellular matrix (ECM)[2] through integrins composed of two subunits (α and β), thereby regulating mast cell functions. As previously reported (5–9), integrins α4β1 and α5β1, or integrin αVβ3, expressed in mast cells mediate binding to fibronectin (FN) or vitronectin (VN), respectively. Interestingly, integrin α4β7 is involved in intestinal homing of mast cell progenitors via interaction with mucosal vascular addressin cell adhesion molecule-1 (10). In view of the implication of mast cell integrins in innate immunity, integrin α2β1 expressed in peritoneal mast cells is required for the induction of inflammatory responses to infection (11). In addition, integrin αVβ6 is essential for nematode-induced mucosal mast cell hyperplasia and for expression of the granule chymase (12).

Integrin αIIb, also known as CD41, which forms a complex with integrin β3, is a well known marker of the megakaryocyte/platelet lineage. Integrin αIIbβ3 is required for normal platelet hemostatic function (13–17). Previously, we reported that integrin αIIbβ3 is also highly expressed in mast cells (9, 18). In addition, we demonstrated that mast cell interaction with fibrinogen (FB) via integrin αIIbβ3 enhances *in vitro* mast cell functions, by using a blocking Ab specific for integrin αIIb (9). On the other hand, higher surface expression levels of integrin αV and enhanced adhesion to VN were found in integrin αIIb-deficient BMMCs as compared with wild-type (WT) counterparts (18), suggesting that integrin αIIb and integrin αV counter-regulate their surface expression levels and functions in mast cells. Therefore, we attempted to carefully analyze the regulatory mechanisms by utilizing retroviral transduction with integrin αIIb WT or non-functional mutant into integrin αIIb-deficient BMMCs.

* This work was supported by grants from the Ministry of Education, Science, Technology, Sports and Culture and the Ministry of Health and Welfare, Japan.

[1] To whom correspondence should be addressed. Tel.: 81-3-5449-5759; Fax: 81-3-5449-5428; E-mail: kitaura-tky@umin.ac.jp.

[2] The abbreviations used are: ECM, extracellular matrix; BMMCs, bone marrow-derived mast cells; FB, fibrinogen; FN, fibronectin; SA, fixed *S. aureus* Cowan I; PCA, passive cutaneous allergic reaction; SCF, stem cell factor; VN, vitronectin; vWF, von Willebrand factor; WT, wild type; Ab, antibody; mAb, monoclonal antibody; IL-3, interleukin-3; BSA, bovine serum albumin; PBS, phosphate-buffered saline; LPS, lipopolysaccharide; TNP, trinitrophenol; DNP, dinitrophenol; WT, wild type; KO, knockout.

FB abundant in plasma contributes to blood clotting (19). In addition, FB as well as its degradation product fibrin are also present in ECM outside blood vessels, where they play important roles in inflammation and wound healing through recruitment and activation of inflammatory cells expressing FB-binding receptors (19–22). Interestingly, surface proteins that bind to FB are also expressed by several types of bacteria, such as *Staphylococcus aureus* and *Streptococcus pyogenes*, which modulate immune responses to bacterial infections (23–25).

In the present study, we showed that integrin αIIb expression levels regulate surface expression levels of integrin αVβ3 as well as integrin αIIbβ3 in mast cells and that mast cell functions augmented by interaction with FB are dependent on integrin αIIbβ3 and independent of integrin αVβ3. In accordance, integrin αIIb deficiency strongly suppressed FB-induced chronic inflammation. Notably, the interaction with soluble FB via integrin αIIbβ3 helps mast cells recognize and respond to *S. aureus* (Cowan I) with FB-binding capacity. Thus, integrin αIIbβ3 in mast cells modulates FB-associated, chronic inflammation and innate immune responses.

EXPERIMENTAL PROCEDURES

Mice—All experimental mice were sex- and age-matched (6–16 weeks old). Balb/c mice were purchased from Charles River Japan (Tokyo, Japan). Integrin aIIb$^{-/-}$ mice were generated as described previously (14) and backcrossed to Balb/c mice for at least six generations. Animal studies were performed according to the guidelines of the animal care committee of the Institute of Medical Science, University of Tokyo.

Antibodies and Other Materials—Source of antibodies (Abs) were as follows: anti-mouse integrin αIIbβ3 mAb (1B5) was a kind gift from Dr. B. S. Coller (Rockefeller University, New York, NY) (26). Anti-mouse integrin αV (8B3) and anti-mouse integrin β3 (8B11) mAbs were kind gifts from Drs. D. J. Gerber and S. Tonegawa (Picower Center, Massachusetts Institute of Technology, Boston, MA) (27). Anti-dinitrophenol (DNP) IgE (SPE-7) was from Sigma. Anti-trinitrophenol (TNP) IgE (C38-2), anti-mouse αIIb (MWReg30), anti-mouse αV (RMV-7 and H9.2B8), anti-mouse α4 (9C10), anti-mouse α5 (5H10–27), anti-mouse LFA1 (M17/4), anti-mouse β1 (Ha2/5), anti-mouse β2 (GAME-46), and anti-αVβ3 (2C9.G2) mAbs and other Abs were from BD Pharmingen. Cytokines such as mouse IL-3 and SCF were obtained from R&D Systems. Bovine serum VN and TNP-conjugated BSA (TNP-BSA) were from Sigma. Human plasma FB and von Willebrand factor (vWF) were from Chemicon. Formalin-fixed *S. aureus* Cowan I was purchased from Calbiochem.

Cells—To generate BMMCs with 95% purity (c-kit$^+$/FcεRI$^+$ by flow cytometry), bone marrow cells from 6-week-old male mice were cultured for 5–8 weeks in the presence of 10 ng/ml IL-3 with or without 20 ng/ml SCF as described previously (9, 28).

DNA Constructs, Transfection, and Infection—To generate mouse integrin αIIb(D163A) mutant, two-step PCR mutagenesis was performed by using mouse integrin αIIb wild-type (WT) cDNA (provided by Dr. R. B. Basani, Children's Hospital of Philadelphia, PA) as a template. Retroviral transfection was as described in a previous study (29). Briefly, integrin αIIb(WT) or αIIb(D163A) mutant cDNA was subcloned into pMXs-IRES-puro^r (pMXs-IP) to generate pMXs-IP-integrin αIIb(WT) or αIIb(D163A), respectively. To generate recombinant retroviruses, pMXs-IP plasmids were transfected into PLAT-E packaging cells (30) with FuGENE 6 (Roche Diagnostics). Cells were infected with retroviruses in the presence of 10 μg/ml Polybrene. Selection with puromycin was started 48 h after infection.

Flow Cytometric Analysis—Cells were stained as described before (9, 28). Cells stained with the indicated Abs were analyzed with a FACSCalibur equipped with CellQuest software (BD Biosciences) and Flowjo software (Tree Star).

Adhesion Assay and Migration Assay—Adhesion assay was done as described (6, 9). In brief, 96-well plates were coated with 20 μg/ml FB, FN, VN, or vWF. BMMCs resuspended at 5×10^5 cells/ml were transferred into coated wells with or without stimulant for 1 h at 37 °C. After washing, cell adhesion was quantitated using CellTiter-Glo™ (Promega, Madison, WI) and a Micro Lumat Plus luminometer (EG&G Berthold), according to the manufacturer's instructions. In assays using blocking Abs, BMMCs were preincubated with 20 μg/ml Abs for 1 h before adding the cells to the plate. Migration assays were carried out as described (7, 9), using 24-well Transwell chambers with 5-μm polycarbonate filters (Corning).

Measurement of Cytokines—The cells were transferred into FB-coated 96-well plates (1×10^4 cells/well) with or without stimulants. After incubating for 12 h at 37 °C, the supernatant of each well was collected, and the concentration of IL-6 or TNF-α was quantified by enzyme-linked immunosorbent assay with OptiEIA for IL-6 or TNF-α (BD Pharmingen) as described (9, 28).

β-Hexosaminidase Release Assay—β-Hexosaminidase release assay was as described before (31). Briefly, 5×10^4 cells of IgE-sensitized BMMCs in Tyrode buffer (10 mM HEPES buffer (pH 7.4), 130 mM NaCl, 5 mM KCl, and 5.6 mM glucose) containing 0.1% BSA, 1 mM $CaCl_2$, and 0.5 mM $MgCl_2$ were stimulated with the indicated concentration of TNP-BSA in BSA- or FB-coated 96-well plates for 1 h at 37 °C. Cell supernatants and total cell lysates solubilized with 1% Nonidet P-40 were collected, and β-hexosaminidase in the supernatants and cell lysates was quantified by spectrophotometric analysis of hydrolysis of *p*-nitrophenyl-*N*-acetyl-β-D-glucopyranoside (Sigma). The percentage of β-hexosaminidase release was calculated.

PCA Reactions—Passive cutaneous anaphylactic (PCA) reactions were performed as described (32–34). Briefly, anti-DNP IgE was intradermally injected into the ears of mice. After 24 h, 250 μg of DNP-BSA and 0.5% Evans blue dye was intravenously injected. The amounts of extravasated dye were measured after 30 min by extracting ears. In another type of experiment, mice received anti-DNP IgE intravenously. After 24 h, a skin reaction was elicited by applying 0.75% dinitrofluorobenzene acetone-olive oil solution to both sides of the ears. The reaction was assessed by measuring the ear thickness 1 h and 12 h after antigen challenge.

FB-induced Chronic Inflammation Model—200 μl of 0.5 mg/ml FB or PBS was intraperitoneally injected into WT or integrin αIIb$^{-/-}$ mice every 2 days. After 1 month, total peritoneal cells of the sacrificed mice were collected by using 3 ml of PBS. Total cell numbers were counted by using a hemocytometer; the percentages of mast cells (c-kit$^+$/FcεRI$^+$), granulo-

cytes (Gr-1^{high}/CD11b$^+$), and macrophages (F4/80$^+$) were calculated by fluorescence-activated cell sorting analysis.

Responses to Fixed S. aureus Cowan I in BMMCs—Fixed *S. aureus* Cowan I (SA) purchased from Calbiochem was stained with Cell Tracker Orange (Molecular Probes). Five × 10^4 BMMCs suspended in 10% BSA/Tyrode buffer were incubated with SA in the presence or absence of 0.5 mg/ml soluble FB in BSA-coated 96-well plates for 2 h. The interaction between mast cells and SA was observed by using a fluorescence microscope. After the supernatant of each well was collected, bacterial cells were removed with a 0.22-μm filter. Cytokine concentrations in the supernatants were quantified by enzyme-linked immunosorbent assay.

Quantitation of Tissue Mast Cells—Tissue mast cells in ear skin, back skin, peritoneal wall, and intestine were quantified by light microscopy at ×400 by an observer who was unaware of the identity (*i.e.* mouse genotype) of the individual specimens, in Giemsa-stained sections, as previously described (28, 35, 36). Results were expressed as mast cells (mean ± S.E.) per mm^2.

Statistical Analysis—Data are shown as the mean ± S.D. Statistical significance was determined by Student's *t* test, with $p < 0.01$ (**) and $p < 0.05$ (*) taken as being statistically significant.

RESULTS

Surface Expression Levels of Integrin αV Are Elevated in Integrin αIIb-deficient BMMCs—To investigate the role of integrin αIIb in mast cells, bone marrow cells from WT and integrin αIIb$^{-/-}$ mice were cultured in the presence of IL-3 for 5 weeks to generate comparable numbers of morphologically pure (>95%) mast cells. BMMCs from WT and integrin αIIb$^{-/-}$ Balb/c mice exhibited similar levels of FcεRI and c-kit on their cell surfaces as determined by flow cytometry (Fig. 1*A*). In addition, proliferative responses to IL-3 as well as apoptosis induced by growth factor (IL-3) deprivation were comparable between both BMMCs (Fig. 1, *C* and *D*). Thus, integrin αIIb deficiency did not affect Balb/c mice-derived mast cell development and growth in suspension culture, as previously reported in C57BL/6 mice (18). Moreover, when IgE-sensitized BMMCs were stimulated with the indicated doses of antigen, we found comparable levels of β-hexosaminidase release and cytokine (IL-6 and TNF-α) production (Fig. 1, *E* and *F*, and data not shown). This also suggested that integrin αIIb deficiency did not modulate FcεRI signaling in suspension culture of mast cells. However, in keeping with previous findings (18), we confirmed the striking differences between the two cell types: surface expression levels of integrin αV and integrin αVβ3 were 10-fold higher in integrin αIIb-deficient BMMCs as compared with WT counterparts, despite comparable expression levels of other integrins such as integrins α4, α5, and β1, and no detectable expression of integrin β2 in either BMMC (Fig. 1*E*). Collectively, these results led us to postulate that integrin αIIb deficiency influenced mast cell functions through interaction with ECM.

Surface Expression Levels of Integrin αV Are Inversely Correlated with Those of Integrin αIIb—We next investigated the mechanism by which surface expression levels of integrin αV were elevated in integrin αIIb-deficient BMMCs. As previously reported (18), mRNA levels of integrin αV and integrin β3 were comparable between WT and integrin αIIb-deficient BMMCs (data not shown), suggesting the post-translational regulation of surface expression levels of integrin αV in BMMCs. Because integrin β3 forms a complex with integrin αIIb or integrin αV, we hypothesized that integrin αV competed with integrin αIIb in the association with integrin β3. To test this, integrin αIIb-deficient BMMCs were retrovirally transduced with integrin αIIb WT or mock. Notably, flow cytometric analysis demonstrated that transduction with integrin αIIb(WT) strongly down-regulated surface expression of integrin αV in integrin αIIb-deficient BMMCs (Fig. 2*A*). In addition, integrin αIIb(D163A) mutant (37), which lost the capacity to bind to FB, was transduced into integrin αIIb-deficient BMMCs. Consistent with a previous report (37), surface expression levels of integrin αIIb(D163A) mutant were weaker than those of integrin αIIb(WT) in the transduced cells. In proportion to less induction of integrin αIIb(D163A), surface expression levels of integrin αV in integrin αIIb(D163A) mutant-transduced cells were less down-regulated as compared with those in integrin αIIb(WT)-transduced BMMCs (Fig. 2*A*). Furthermore, similar experiments were performed using murine T cell lymphoma cell line BW5147, which originally expressed integrin αVβ3 but not integrin αIIbβ3. As shown in Fig. 2*B*, transduction with integrin αIIb(WT) into BW5147 cells down-regulated surface expression of integrin αV to a greater degree as compared with transduction with integrin αIIb(D163A) mutant. Collectively, surface expression levels of integrin αV were inversely related to those of integrin αIIb, and even non-functional integrin αIIb competed with integrin αV for integrin β3.

Reduced Adhesion to FB and Enhanced Adhesion to VN and vWF in Integrin αIIb-deficient BMMCs—Next, we examined the effects of integrin αIIb deficiency on mast-cell adhesion to ECM proteins such as FN, FB, VN, and vWF. IgE stimulation-dependent adhesion to FB was strongly suppressed in integrin αIIb-deficient BMMCs, whereas adhesion to VN or vWF was drastically enhanced in integrin αIIb-deficient BMMCs, presumably because of increased surface expression of integrin αVβ3 in integrin αIIb-deficient BMMCs when compared with WT BMMCs (Fig. 3*A*). On the other hand, integrin αIIb deficiency did not significantly affect the adhesion to FN (Fig. 3*A*). In addition, we examined the inhibitory effect of pretreatment with blocking Abs against integrin αIIbβ3 or integrin αVβ3 on mast-cell adhesion to ECM proteins, confirming that, in WT BMMCs, the binding to FB, VN, or vWF was dependent on integrin αIIbβ3, integrin αVβ3, or both (Fig. 3*B*). Similar experiments were also performed with regard to integrin αIIb-deficient BMMCs, demonstrating that pretreatment with blocking Abs against integrin αV dampened IgE stimulation-dependent strong adhesion to VN or vWF as well as weak adhesion to FB, whereas it did not affect the adhesion to FN (Fig. 3*B*). In contrast, pretreatment with blocking Ab for integrin αIIb did not reduce the adhesive property at all (Fig. 3*B*). Collectively, these results suggested that elevated surface expression levels of integrin αVβ3 in αIIb-deficient BMMCs enhanced the adhesion to VN or vWF, but it did not compensate for the defective adhesion to FB owing to integrin αIIbβ3 deficiency.

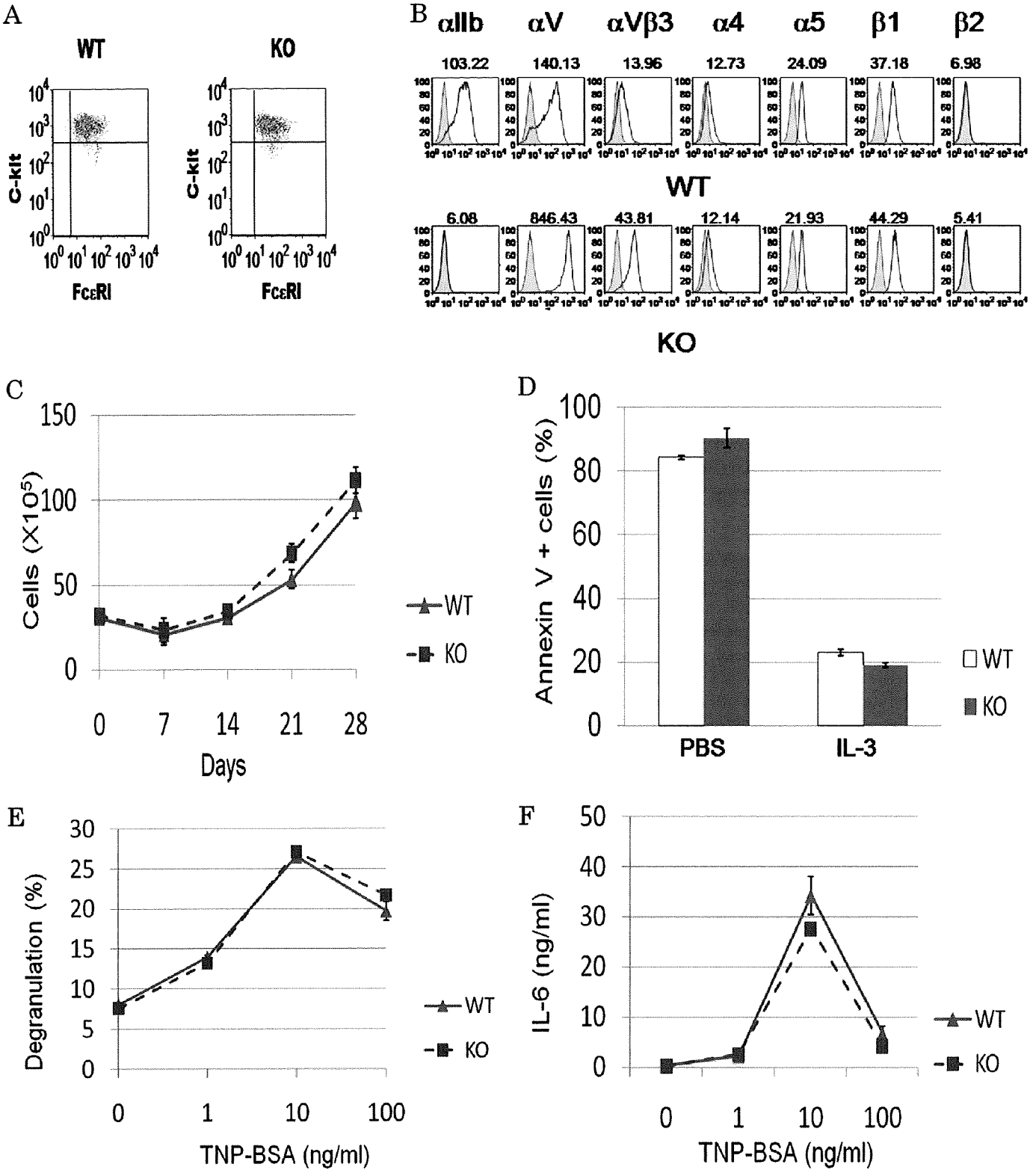

FIGURE 1. **Functional analysis of WT and integrin αIIb-deficient BMMCs in *in vitro* suspension culture.** *A* and *B*, surface expression levels of FcεRI and c-kit as well as several integrins such as integrin αIIb, αV, αVβ3, α4, α5, β1, and β2 in WT and integrin αIIb-deficient BMMCs. Mean fluorescent intensities of staining were indicated. Data are representative of three independent experiments. *C*, *in vitro* growth curves of bone marrow cells derived from WT and integrin αIIb-deficient mice. Numbers of trypan blue-excluding cells in bone marrow cell cultures in IL-3-containing medium were counted weekly. Data are representative of three independent experiments. All data points correspond to the mean ± S.D. *D*, IL-3 deprivation-induced apoptosis of WT and integrin αIIb-deficient BMMCs. Percentage of annexin V-positive cells after 48 h was measured by flow cytometric analysis. Data represent three independent experiments. All data points correspond to the mean ± S.D. *E* and *F*, after IgE-sensitized WT and integrin αIIb-deficient BMMCs were stimulated with the indicated concentrations of antigen for 50 min or 24 h, the amounts of β-hexosaminidase (*E*) or IL-6 (*F*), respectively, released into medium were measured. Data represent three independent experiments. All data points correspond to the mean ± S.D.

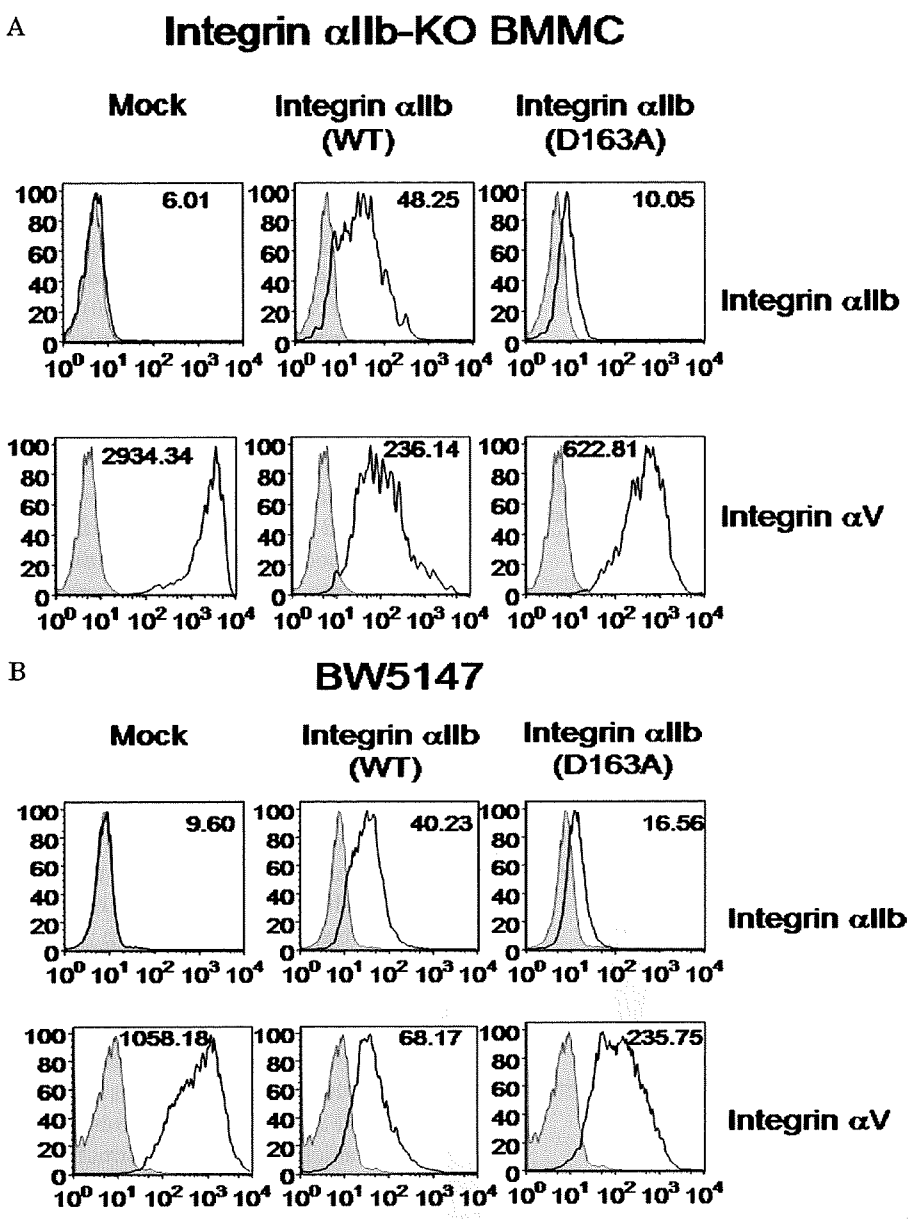

FIGURE 2. **Elevated surface expression levels of integrin αV in integrin αIIb-deficient BMMCs were reduced by transduction with integrin αIIb.** *A* and *B*, integrin αIIb-deficient BMMCs (*A*) or BW5147 cells (*B*) were transduced with integrin αIIb(WT), αIIb(D163A) mutant, or mock. Surface expression levels of integrin αIIb or integrin αV in these transfectants were analyzed by flow cytometry. Mean fluorescent intensities of staining were indicated. Data represent three independent experiments.

specific ligand for integrin αIIbβ3. Moreover, it was found in WT, but not integrin αIIb-deficient, BMMCs that SCF-stimulated mast-cell proliferation was accelerated in FB-coated plates as compared with BSA-coated plates (Fig. 4*A*). Similarly, when stimulated by IgE plus antigen, WT, but not integrin αIIb-deficient, BMMCs enhanced β-hexosaminidase release and cytokine (IL-6 and TNF-α) production through interaction with FB (Fig. 4, *B–D*). Altogether, integrin αIIbβ3 plays crucial roles in enhancing mast-cell functions through interaction with FB.

Transduction with Integrin αIIb-(WT), but Not Integrin αIIb(D163A) Mutant, into Integrin αIIb-deficient BMMCs Recovered Mast Cell Functions through Interaction with FB—To further reduce the possibility that enhanced expression levels of integrin αVβ3 modulated mast-cell functions through interaction with FB, we performed similar experiments on adhesion and cytokine production in integrin αIIb-deficient BMMCs transduced with integrin αIIb(WT), integrin αIIb-(D163A) mutant, or mock. As depicted in Fig. 5*A*, transduction with integrin αIIb(WT), but not integrin αIIb(D163A) mutant, augmented the adhesion to FB as compared with transduction with mock. On the other hand, transduction with integrin αIIb(D163A) as well as integrin αIIb(WT) diminished the adhesion to VN, with the degree of the former being a little lower than that of the latter, which was consistent with surface expression levels of integrin αVβ3 in integrin αIIb-deficient BMMCs transduced with integrin αIIb(WT) and (D163A) mutant (Fig. 2*A*). Moreover, transduction with integrin αIIb(WT), but not integrin αIIb(D163A), induced the enhancement of cytokine production through interaction with FB in integrin αIIb-deficient BMMCs (Fig. 5*B*). Collectively, these results definitively confirmed that enhanced mast cell functions through interaction with FB were dependent on integrin αIIbβ3 but not integrin αVβ3.

Enhancement of Migration, Proliferation, Degranulation, and Cytokine Production of BMMCs through Interaction with FB Is Dependent on Integrin αIIb—We next examined the effect of integrin αIIb deficiency on mast-cell functions through interaction with FB. As previously reported, SCF induced migration of WT BMMCs when the lower membranes of the Transwells were pre-coated with FB, FN, or VN. Comparison of the migrating cell numbers between WT and integrin αIIb-deficient BMMCs revealed that integrin αIIb deficiency strongly diminished or enhanced the migration of BMMCs through interaction with FB or VN, respectively, whereas it did not affect mast cell migration through interaction with FN (Fig. 3*C*). These results also suggested that, in integrin αIIb-deficient BMMCs, both the adhesive and migratory ability were altered toward integrin αVβ3, whereas there was little interaction with FB, a

Integrin αIIb Deficiency Affected Neither Tissue Mast Cell Numbers in Steady States nor Mast Cell-mediated Acute Allergic Reactions—Because enhanced proliferation and migration of BMMCs through interaction with FB were suppressed by integrin αIIb deficiency, we compared the quantity of tissue mast cells in WT and in integrin $\alpha IIb^{-/-}$ mice. Microscopic

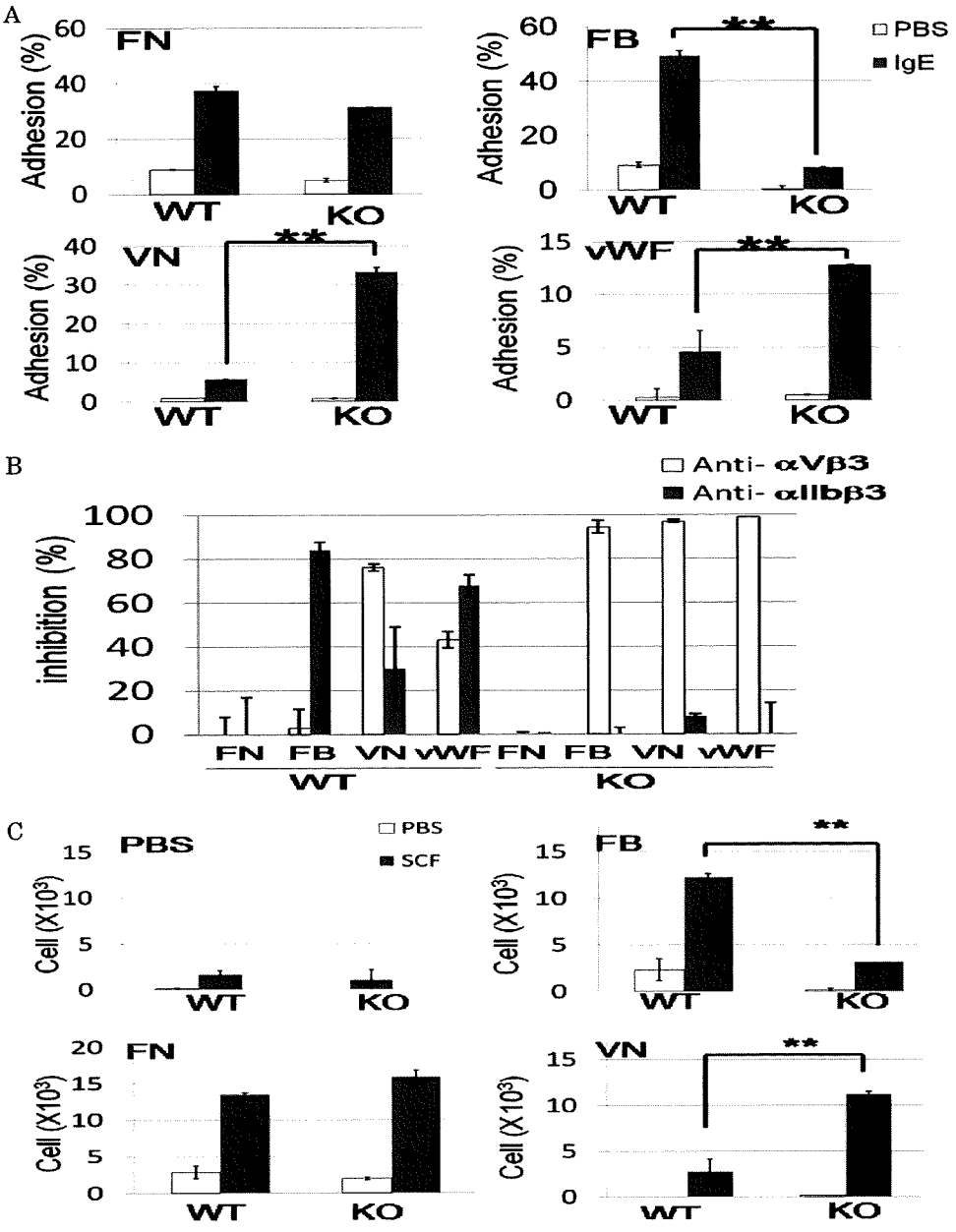

FIGURE 3. **Enhanced adhesion to VN or vWF and deteriorated adhesion to FB in integrin αIIb-deficient BMMCs.** *A*, WT and integrin αIIb-deficient BMMCs were incubated with or without 5 μg/ml SPE-7 IgE in FN-, FB-, VN-, or vWF-coated plates. Percentage of adherent cells was measured. Data are representative of three independent experiments. All data points correspond to the mean ± S.D. ** ($p < 0.01$) and * ($p < 0.05$) indicate statistical differences. *B*, pretreatment with blocking Ab for integrin αIIb or integrin αV inhibited to various degrees the adhesion of WT- or integrin αIIb-deficient BMMCs stimulated by 5 μg/ml IgE in FN-, FB-, VN-, or vWF-coated plates. Percentage of inhibition was measured. Data are representative of three independent experiments. All data points correspond to the mean ± S.D. *C*, WT or integrin αIIb-deficient BMMCs in the upper wells were attracted by 100 ng/ml SCF in the lower wells through BSA-, FB-, FN-, or VN-coated Transwells. Migrated cells were counted. Data represent three independent experiments. All data points correspond to the mean ± S.D. ** ($p < 0.01$) indicates statistical differences.

analysis demonstrated that mast-cell numbers in the ear skin, back skin, peritoneum wall, and small intestine were not different in these mice (Table 1). Based on this, we addressed the question of whether tissue FB extravasated by acute inflammation modulated mast cell-associated allergic reactions of WT and integrin $\alpha IIb^{-/-}$ mice. However, no significant difference of two types of PCA reaction was observed in these mice (data not shown), despite enhanced *in vitro* degranulation and cytokine production of mast cells through integrin αIIbβ3-dependent interaction with FB (Fig. 4, *B–D*). These results indicated that integrin αIIbβ3 was not involved in tissue mast-cell numbers and distributions in steady states or IgE-mediated acute allergic responses.

Integrin αIIb Deficiency Suppressed Peritoneal Chronic Inflammation with a Remarkable Increase of Mast Cells Induced by Repetitive Intraperitoneal FB Administration—We next asked whether integrin αIIb deficiency influenced chronic inflammation with extravascular FB and fibrin deposition. To explore the direct effects of FB, we adopted FB-induced chronic inflammation models where FB was administered into peritoneal cavities every other day. After 1 month, we counted total peritoneal cell numbers and estimated cell populations by flow cytometric analysis. In steady states before the stimulation, we found no significant differences in total peritoneal cell numbers or in mast cell numbers between WT and integrin $\alpha IIb^{-/-}$ mice (Fig. 6*A* and data not shown). Interestingly, repetitive intraperitoneal injection of FB, but not PBS as a control, induced severe chronic inflammation with a remarkable increase of mast cells as well as total inflammatory cells in the peritoneal cavities of WT mice (Fig. 6, *A* and *B*). Thus, an FB-induced chronic inflammation model was established. Intriguingly, integrin αIIb deficiency strongly suppressed the number of mast cells as well as the total number of inflammatory cells in the peritoneal cavities (Fig. 6, *A* and *B*), although the percentages of granulocytes and macrophages were not significantly different in the WT and integrin $\alpha IIb^{-/-}$ mice (Fig. 6*B*, *right panel*). Considering the *in vitro* roles of mast cell integrin αIIβ3-FB interaction, these results strongly suggested that *in vivo* FB-induced chronic inflammation was largely dependent on integrin αIIbβ3 in mast cells, although the effect of few, if any, platelets in the peritoneal cavities on this phenomenon was not completely ruled out. In addition, we found comparable numbers of inflammatory cells in WT and integrin αIIb-deficient mice 24 h after single dose of FB injection (data not shown). Therefore, FB-induced chronic inflammation required continuous administration of FB. Collectively, integrin αIIbβ3 in mast cells played

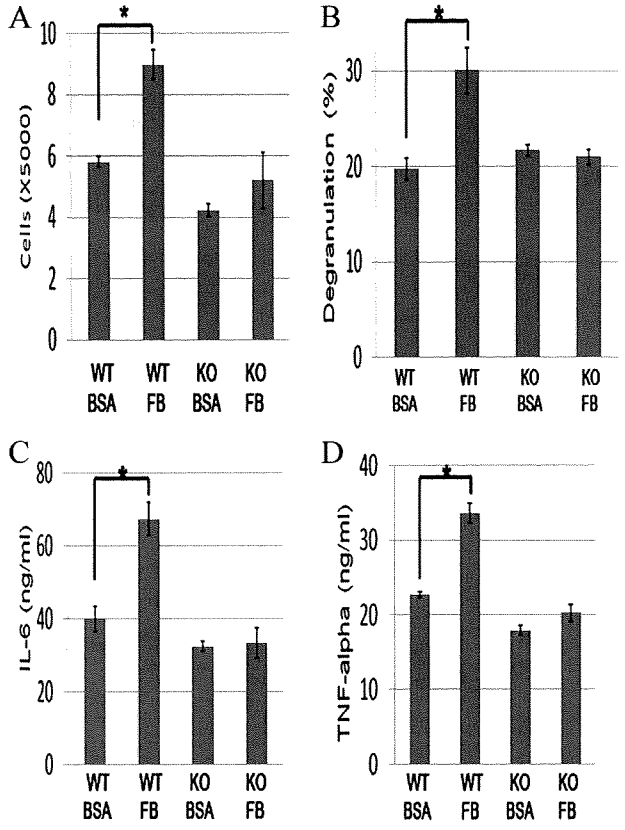

FIGURE 4. **Enhanced proliferation, degranulation, and cytokine production of WT, but not integrin αIIb-deficient, BMMCs through interaction with FB.** *A*, cell numbers of WT or integrin αIIb-deficient BMMCs stimulated by 10 ng/ml IL-3 plus 100 ng/ml SCF for 5 days in BSA- or FB-coated plates. *B*, β-hexosaminidase release of IgE-sensitized WT or integrin αIIb-deficient BMMCs stimulated by 30 ng/ml TNP-BSA for 60 min in BSA- or FB-coated plates. *C* and *D*, IL-6 (*C*) and TNF-α (*D*) production of IgE-sensitized WT or integrin αIIb-deficient BMMCs stimulated by 30 ng/ml TNP-BSA for 16 h in BSA- or FB-coated plates. All data are representative of four independent experiments. All data points correspond to the mean ± S.D. * ($p < 0.05$) indicates statistical differences.

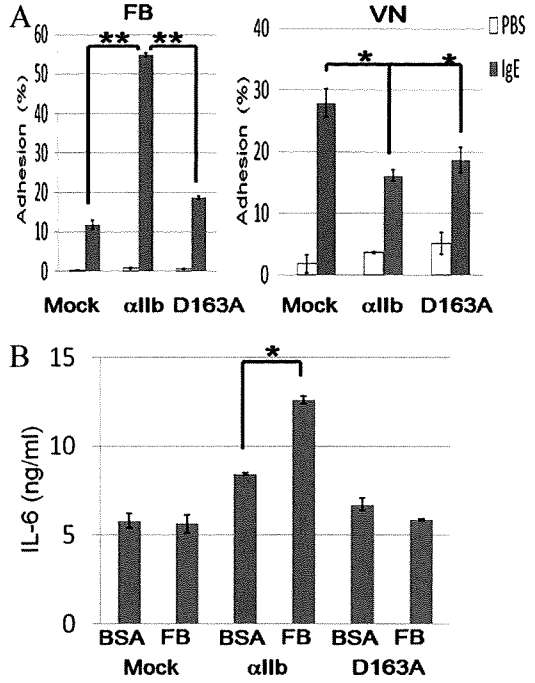

FIGURE 5. **Transduction with integrin αIIb(WT) enhanced or suppressed the adhesion to FB or VN, respectively, in integrin αIIb-deficient BMMCs.** *A*, integrin αIIb-deficient BMMCs transduced with integrin αIIb(WT), αIIb(D163A) mutant, or mock were incubated with 5 μg/ml SPE-7 IgE for 60 min in FB- or VN-coated plates. The percentage of adherent cells was measured. Data are representative of three independent experiments. All data points correspond to the mean ± S.D. ** ($p < 0.01$) and * ($p < 0.05$) indicate statistical differences. *B*, integrin αIIb-deficient BMMCs transduced with integrin αIIb(WT), αIIb(D163A) mutant, or mock were incubated with 5 μg/ml SPE-7 IgE for 16 h in FB-coated plates. The amounts of IL-6 released into medium were measured. Data are representative of three independent experiments. All data points correspond to the mean ± S.D. * ($p < 0.05$) indicates statistical differences.

TABLE 1

Numbers of mast cells in ear skin, back skin, peritoneum wall, and small intestine

Numbers of mast cells per ten randomly selected high power fields were determined under light microscopy. Results are the mean values ± S.E. for four mice/group. WT, wild type; KO, knockout.

Tissue	WT	KO
Ear skin	112 ± 11.7	109 ± 3.2
Back skin	29.7 ± 23	41.3 ± 13
Peritoneum wall	9.3 ± 5.0	10 ± 2
Small intestine	5.3 ± 3.3	6 ± 3.0

an important role in FB-mediated chronic, but not acute, inflammatory responses.

Soluble FB Enhanced Cytokine Production of WT, but Not Integrin αIIb-deficient BMMCs, in Response to S. aureus Cowan I with FB-binding Capacity—As previously reported, mast cells adhered to soluble FB as well as plate-coated FB via integrin αIIbβ3. Because soluble FB is bound by certain types of bacteria such as *S. aureus* (Cowan I), the immune cells expressing FB-binding receptors are thought to modulate the immune responses to these pathogens (23–25). We then investigated whether soluble FB influenced the response of mast cells to *S. aureus* (Cowan I). When WT or integrin αIIb-deficient BMMCs were incubated with *S. aureus* (Cowan I) for 2 h in the presence of soluble FB, fluorescent microscopic analysis demonstrated that WT, but not integrin αIIb-deficient, BMMCs were completely surrounded by aggregated *S. aureus* (Cowan I) probably through interaction with soluble FB (Fig. 7*A*). On the other hand, BMMCs were not apparently covered with *S. aureus* (Cowan I) in the absence of soluble FB. These results suggested that integrin αIIbβ3-dependent interaction of BMMCs with *S. aureus* (Cowan I) via soluble FB probably helped mast cells recognize this pathogen. Moreover, IL-6 released into each supernatant was quantified by enzyme-linked immunosorbent assay, demonstrating that soluble FB-induced enhancement of IL-6 production was observed only in WT, but not integrin αIIb-deficient, BMMCs in response to *S. aureus* (Cowan I) (Fig. 7*B*). To examine the specificity of this phenomenon, similar experiments were performed using *Escherichia coli* without FB-binding capacity. As shown in Fig. 7*B*, soluble FB-dependent enhancement of IL-6 production of BMMCs stimulated by *E. coli* was not observed irrespective of integrin αIIb expression, suggesting that soluble FB induced the enhancement of cytokine production of BMMCs in response to bacteria with, but not without, FB-binding capacity. Because Toll-like receptors primarily play an important part in the recognition of and response to bacteria (3), we also asked if soluble FB or immobilized FB enhanced cytokine production of both BMMCs stimulated by LPS, a Toll-like receptor 4 agonist. As

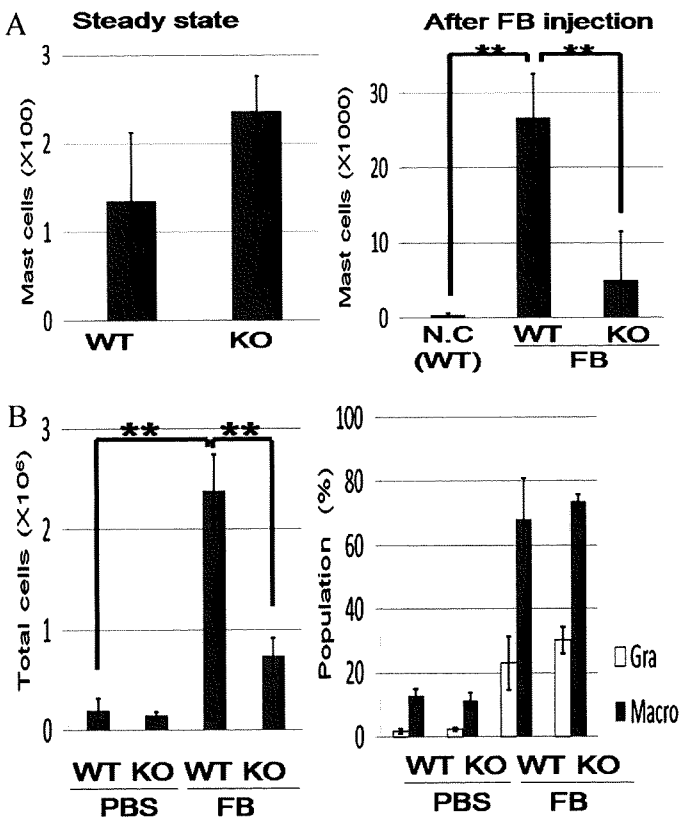

FIGURE 6. **Repetitive injection of FB into peritoneal cavities induced chronic inflammation more severely in WT mice in comparison to integrin αIIb-deficient mice.** *A*, peritoneal mast cell numbers of WT and integrin αIIb-deficient mice before (*left panel*) and after (*right panel*) FB injection. *B*, total peritoneal cell numbers (*left panel*) and cell populations (*right panel*) of WT and integrin αIIb-deficient mice after continuous intraperitoneal inoculation of FB or PBS for 1 month ($n = 5$/genotype). All data points correspond to the mean ± S.D. ** ($p < 0.01$) indicates statistical differences.

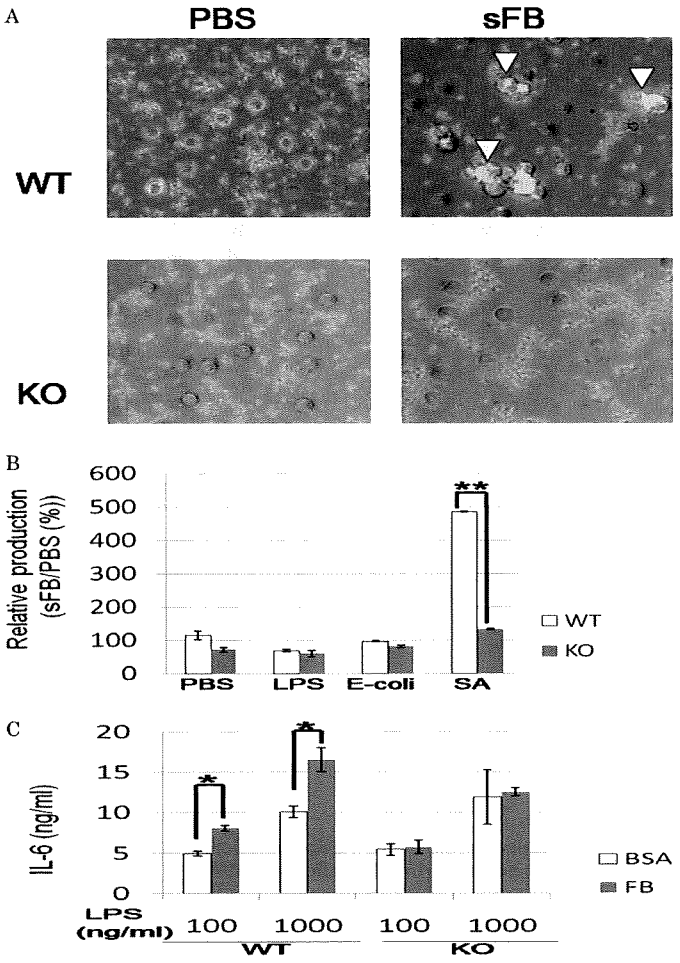

FIGURE 7. **Soluble FB enhanced cytokine production of WT, but not integrin αIIb-deficient, BMMCs in response to *S. aureus* with FB-binding capacity.** *A*, WT or integrin αIIb-deficient BMMCs were incubated with heat-killed *S. aureus* labeled by Cell Tracker Orange in the presence or absence of 500 μg/ml soluble FB for 2 h. WT, but not integrin αIIb-deficient, BMMCs were covered with SA aggregates in the presence of soluble FB (*arrowhead*). *B*, WT or integrin αIIb-deficient BMMCs were incubated with 100 ng/ml LPS, 100 μg/ml heat-killed *E. coli*, 100 μg/ml *S. aureus*, or PBS as control in the presence or absence of 500 μg/ml soluble FB for 8 h. The ratio of the amounts of IL-6 released in the presence of soluble FB to those of IL-6 in the absence of soluble FB was measured. Data are representative of three independent experiments. All data points correspond to the mean ± S.D. ** ($p < 0.01$) indicates statistical differences. *C*, WT or integrin αIIb-deficient BMMCs were incubated with the indicated concentrations of LPS in FB- or BSA-coated plates. Data represent three independent experiments. All data points correspond to the mean ± S.D. * ($p < 0.05$) indicate statistical differences.

depicted in Fig. 7 (*B* and *C*), soluble FB did not affect IL-6 production of either WT or integrin αIIb-deficient BMMCs stimulated by LPS, whereas immobilized FB enhanced IL-6 production of WT, but not integrin αIIb-deficient, BMMCs stimulated by LPS. These results suggested the synergism of Toll-like receptor 4 signaling and integrin αIIbβ3 signaling through interaction with immobilized FB, but not soluble FB. Altogether, soluble FB enhances the cytokine production of BMMCs in responses to *S. aureus* (Cowan I), probably because mast cell-soluble FB-*S. aureus* (Cowan I) complex formation promoted the quick and tight recognition of this pathogen by mast cells.

DISCUSSION

In a previous study, we found that integrin αIIbβ3 is highly expressed in mast cells, in addition to the megakaryocyte/platelet lineage and a subset of hematopoietic progenitors (9, 14, 18). Experiments using blocking Abs specific for integrins demonstrated that adhesion to FB, VN, or vWF was mediated through integrin αIIbβ3, integrin αVβ3, or both, respectively (9). In the follow-up study, we first paid attention to the interesting results shown by Berlanga O *et al.* that integrin αIIb-deficient BMMCs displayed extremely higher surface expression levels of integrin αVβ3 as compared with WT counterparts (18). Because counter-regulation of integrin αIIbβ3 and integrin αVβ3 on their surface expression levels might affect *in vivo* functions of integrin αIIbβ3 in mast cells, we attempted to delineate the underlying mechanism. Our hypothesis that integrin αIIb competed with integrin αV in heterodimerization with integrin β3 in mast cells was illustrated by experimental results as follows: retroviral transduction with integrin αIIb(WT) into integrin αIIb-deficient BMMCs reduced surface expression of integrin αVβ3 at levels comparable to those in WT BMMCs (Fig. 2*A*). In addition, transduction with integrin αIIb(D163A) mutant led to less reduction in surface expression levels of integrin αVβ3 together with less induction in those of integrin αIIbβ3 in integrin αIIb-deficient BMMCs. Thus, surface expression levels of integrin αVβ3 were conversely related to those of integrin αIIbβ3 in mast cells (Fig. 2*A*). Notably, this phenomena was true for BW5147 cells transduced with integrin αIIb(WT) or